POLITECNICO DI TORINO

Master's Degree in Biomedical Engineering

Master's Degree Thesis

Targeted Nanoparticles for synergistic drug delivery to Multiple Myeloma

Supervisor:
Prof. Valentina Cauda

Candidate:
Giada Rosso

Academic year 2020/2021

July 2021

Abstract

In the latest years, nanomedicine has gained immense attention, providing promising and innovative therapeutic strategies. This is particularly true for nanosystems employed in cancer treatment, by virtue of the small size of devices and their easily tunable physical and morphological properties, which allow effective interactions at a molecular level with cells. In the present Master Thesis, the purpose is to develop a biomimetic protocell, namely a drug-loaded nanosystem which, thanks to its surface functionalization, is capable to selectively address, be internalized and kill cancer cells, avoiding the typical side-effects associated with conventional therapies. The nanoconstructs are specifically designed to target Multiple Myeloma (MM). In particular, they were designed with a Mesoporous Silica Nanoparticle (MSN) core, which is covered with a self-assembled lipidic double layer (shell), necessary to enhance biostability and functionalization. Mesoporous silica is a highly biocompatible material, and it is characterized by a huge specific surface area (approximately 1000 m^2/g) which allows to encapsulate a great amount of drug molecules. In this project, the MSNs were synthetized using a template-assisted sol-gel self-assembly process, obtaining 40-50 nm sized nanoparticles and a mesoporous structure characterized by cylindrical and uniform (3-4 nm) pores. The mesoporous structure was exploited to adsorb and encapsulate a highly water-insoluble drug, AGI-6780, otherwise impossible to administer due to its great hydrophobicity and extremely poor biodistribution properties. AGI-6780 is not lethal for the cells itself; however, it was proven to synergize with Carfilzomib (CFZ), a common chemotherapeutic drug currently used in clinics, to which patients often develop resistance. In this Master Thesis, strong effort was made in relation to drug loading, trying to enhance drug loading efficiency with different uptake solutions and concentrations. Another crucial step was the decoration of the surface of the nanocarrier with antibody fragments. Since MM cancer cells overexpress CD38 receptor, anti-CD38 monoclonal antibody was chosen for functionalization, allowing a highly specific and selective interaction between MM cells and NPs. Different antibody-lipids coupling methods were tested and qualitatively evaluated by means of fluorescence microscopy. The therapeutic efficacy of the developed nanoconstructs and contextually the synergy between AGI-6870-loaded MSNs and CFZ were tested on a Human Multiple Myeloma cell line by Molecular Biotechnology Center (MBC, University of Turin).

Contents

List of Tables

List of Figures

1 State of Art

1.1 Multiple Myeloma

Multiple myeloma (MM) is the second most common hematological malignancy (after non-Hodgkin Lymphoma) affecting approximately 6000 new patients every year in Italy and representing 1,3% of the totality of cancers in women and the 1,2% for men [1]. MM originates from Lymphocytes B and plasma cells, which reside primarily in the bone marrow (BM). Plasma cells (PCs) synthetize and release antibodies, having thus an essential role in the immune response. The malignancy is characterized by their uncontrolled proliferation in the BM, interfering with the normal growth of other blood cells and causing the dysregulation of the immune system. The distinctive characteristic of MM is the abnormal production of protein M (monoclonal immunoglobulin), a non-functional monoclonal immunoglobulin, which can be found in the patient's serum.
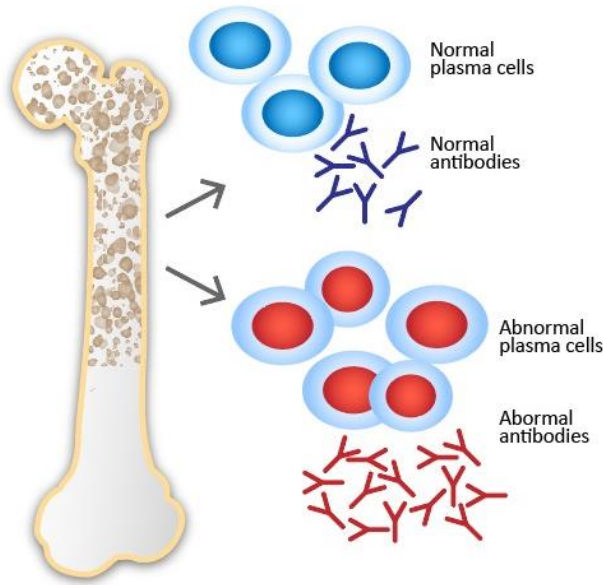
Figure 1.1 *MM is a malignancy affecting plasma cells in the bone marrow. Malignant cells produce massive quantities of monoclonal immunoglobulins (protein M).*

The production and accumulation of protein M in tissues and organs, together with other cytokines secreted by the malignant cells, cause the typical complications associated with MM such as bone lesions and pathological fractures, kidney failure, hypercalcemia and anemia. These are known as C.R.A.B. features [2]:

C → Calcium (hypercalcemia): malignant PCs secrete cytokines that stimulate osteoclast. Consequently, the equilibrium between old bone resorption action by osteoclasts and new bone building action by osteoblasts in the bone remodeling process is unbalanced. This leads to bone weakening and loss and subsequently to the enhancement of calcium levels in blood.

R → Renal Failure: Malignant PCs produce great amounts of immunoglobulins and other abnormal proteins, whose accumulation in the kidney can cause damage. Hypercalcemia contributes to kidney failure as well.

A → Anemia: the abnormal growth and proliferation of infiltrating PCs in the bone marrow inhibits the production of red blood cells.

B → Bone lytic lesions: as discussed before, higher levels of resorption cause bone weakening, leading to bone pain and eventually to fractures. The most affected areas are the spine and the ribs.

"CRAB" SYMPTOMS FOR ACTIVE MYELOMA

| C = high calcium | R = renal problems | A = anemia | B = bone problems |

Figure 1.2 *typical symptoms of active myeloma*

C.R.A.B. features are only the most common clinical manifestation of the disease but patients present a variety of other symptoms and clinical outcomes; in fact MM is extremely heterogeneous both clinically and biologically [3]. Nowadays the causes and the mechanisms underlaying MM are still unclear; it is however believed to be not uniquely but strongly connected to a series of disorders referred to as monoclonal gammopathies, which often precede the development of the malignancy [4]. In particular, monoclonal gammopathy of undetermined significance (MGUS), is an asymptomatic disorder, characterized by the production of monoclonal protein by PCs infiltrated in the bone marrow. MGUS is considered a risky condition, as in approximately 15% cases it represents the precursor state of MM. [2]

The investigation of the monoclonal gammopathies mechanisms and the steps dictating the transition from MGUS to MM is essential for understanding the development of the malignancy. Plasma cells differentiate from hematopoietic stem cells, which undergo a multistage differentiation in the BM and in secondary lymphoid organs, following the lymphoid differentiation path and becoming firstly a Pro-B cells, Pre-B cells and then immature B cells. In the bone marrow, B cells mature, rearranging their membrane and exposing on the surface particular receptors. Depending on the receptors (i.e. IgH-IgL complex) expressed, the mature B cells can migrate towards different body districts, leaving the bone marrow and circulating in the blood stream. Once mature, B cells can eventually differentiate in Plasma cells or Memory cells [5]. Several genetic alterations were found to be associated to the MGUS pre-malignant condition and to MM itself. In particular, the most common primary alteration connected to MM pathogenesis is a chromosomal translocation that involves the immunoglobulin heavy chain (IgH) locus.[6]
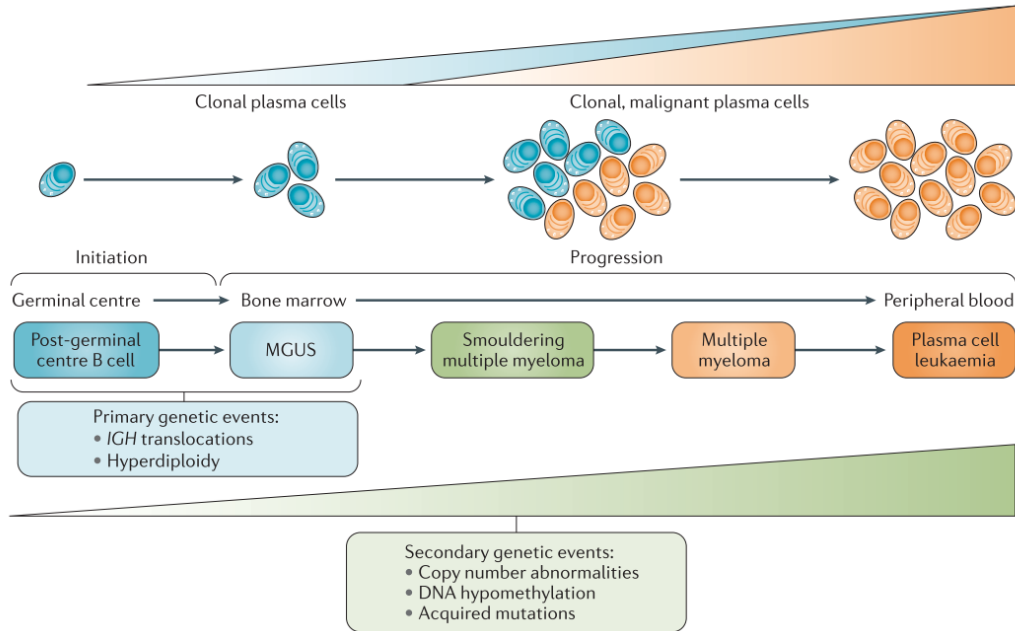
Figure 1.3 *Development of MM from monoclonal gammopathies* [2]

Although MM is still uncurable, the therapies and the prognosis of MM have substantially changed during the past two decades and there are currently several classes of drugs available for the treatment of the newly diagnosed and relapsed malignancy (see Table 1.1 *Currently employed drugs in MM treatment.*).

Conventional chemotherapeutical drugs, (Melphalan, Cyclophosphamide, Predni-sone and Doxorubicin) have begun to be replaced by innovative non-chemothera-peutic agents, such as immunomodulatory drugs and the Proteasome Inhibitors. Unfortunately, these novel agents do not lack side effects but the consequences on the organism are quite different from those seen for standard chemotherapeutic treatment. The different toxicity profiles allow to alternate and combine the ther-apies, with the aim of enhancing the efficacy of the treatment and avoiding cumu-lative toxicities [7]. Particularly used nowadays, since it is one of the most effective, is the combination between immunomodulatory drugs with proteasome inhibitors, such as Bortezomib (BTZ) and Carfilzomib (CFZ) [2].

Table 1.1 *Currently employed drugs in MM treatment.*

Alkylating agents	• Melphalan • Cyclophosphamide • Bendamustine
Proteasome inhibitors (PIs)	• Bortezomib (BTZ) • Carfilzomib (CFZ) • Ixazomib
Immunomodulatory drugs (IMiDs)	• Thalidomide • Lenalidomide • Pomalidomide
Monoclonal antibodies	• Daratumumab (anti-CD38) • Elotuzumab (anti-SLAMF7)
Histone deacetylase inhibitor	• Panobinostat
Others	• Dexamethasone • Prednisone • Cisplatin • Etoposide • Doxorubicin

All the mentioned therapies (both traditional and innovative ones) carry the burden of side effects at systemic level, lacking indeed of targeting capabilities. In order to overcome this limitation, novel therapies such as immunotherapy or immune oncology were widely studied and applied. The concept of immunotherapy is the artificial stimulation of the native immune system against tumoral cells. The sensibilization of the immune system can be achieved by different means including cancer vaccines, oncolytic virus therapy, immunomodulators, adoptive cells therapies and targeted antibodies. These types of solution have gained immense attention in the last decade and several immunotherapy-based drugs reached FDA approval. From the targeted antibodies family, monoclonal antibodies are the most diffused and exploited also in the present work. In fact, monoclonal antibodies have the ability to selectively target the malignant cells, recognizing specific or overexpressed tumor receptors [8],[9].

Nevertheless, none of the above-cited oncological treatments, neither alone nor in combination, has shown to be satisfactorily effective against MM: refractory MM is still highly frequent, with over 90% of relapse rate and median overall survival of approximately 3 years [10].

In this work, as previously mentioned, it is explored a novel drug combination, between the proteasome inhibitor Carfilzomib and another drug, AGI-6780, described in the following paragraphs, together with a nano-sized delivery strategy, that includes the use of monoclonal antibodies exposed on the surface of the nanocarrier, in order to achieve selective targeting of the malignant cells. The used therapeutical agents and targeting strategies are discussed in detail as follows.

The Proteasome and Proteasome Inhibitors

The introduction of the Proteasome inhibitors, with the FDA approval in 2003 of Bortezomib, gave the birth of a new therapeutic strategy: BTZ, in fact, emerged for its efficacy in combined therapies, reaching significant results in clinical trials, in combination with immunomodulatory drugs, monoclonal antibodies and small molecules. Although BTZ demonstrated good results in clinical trials, many patients develop resistance to it after the first cycles of chemotherapy. Additionally,

BTZ was found to be responsible of severe adverse events, such as peripheral neuropathy [11].

To overcome these drawbacks, a second generation of PIs was developed: Carfilzomib and Ixazomib were approved and integrated in both salvage and frontline therapy regimens, increasing the overall survival. However, also second generation of PIs showed dangerous side effects. In particular, CFZ is associated to cardiac toxicity, provoking hypertension, dyspnea and cardiac failure in a higher percentage of patients compared to BTZ [12] [13]. Despite these downsides, PIs are currently routinely administered in clinical settings due to their efficacy in several regimens with other cytotoxic agents [11].

The reason for the success of bortezomib and other proteasome inhibitors is attributable to the huge sensitivity of MM cells to the inhibition of 26S proteasome, capable of degrading the majority of polypeptides in the cytoplasm [13]. Since plasma cells produce antibodies (namely they are protein-producing cells) and malignant PCs in particular produce massive quantities of protein M, stresses on protein turnover mechanism can be detrimental for them [2]. Proteasome inhibition leads in fact to protein overload and stresses the endoplasmic reticulum, eventually driving cells to apoptosis [13].

Proteasome is a multi-subunit and highly sophisticated protein complex, present in the nucleus and in the cytoplasm of all eukaryotic cells [14]. It is part of the Ubiquitin-Proteasome-system (UPS), essential for the maintenance of cell homeostasis, since it is responsible of the degradation of regulatory and short-lived signaling peptides as well as misfolded, redundant and structurally aberrant proteins [13]. 26S proteasome is a 2,5MDa multi-catalytic complex composed by a cylindric core, known as 20S proteasome, in charge of the catalytic break-down of the target protein, and one or two 19S regulatory subunit. The degradation of the proteins (Figure 1.4) by UPS is a multi-stage, highly selective mechanism, in which various enzymes are involved, in order to allow the exclusive destruction of the unwanted proteins. The process starts with ubiquitination: the proteins destined to be destroyed are marked with a chain of polymerized ubiquitin. Ubiquitin is a key molecule in the degradation of proteins, as it selectively binds to the target thanks to the mediation of a series of enzymes including E1, *(ubiquitin-activating), E2 (ubiquitin-conjugating) and E3 (ubiquitin-ligating)*. The polymerization of ubiquitin

(with the formation of a chain with more than 4 units of ubiquitin) is a sentence of death for the target protein: the ubiquitin chain marks and shutters the unwanted protein to the 19S subunit, where it is unfolded and transferred into the 20S catalytic core. Here the target protein is sequentially degraded, producing oligopeptides composed by 3 to 15 amino acid residues, that are subsequently hydrolyzed in single amino acids by peptidases (oligopeptidases or amino-carboxyl peptidases). Both ubiquitin and the amino acids that can be recycled; amino acids are reused by the cell as building blocks to produce new proteins [15].
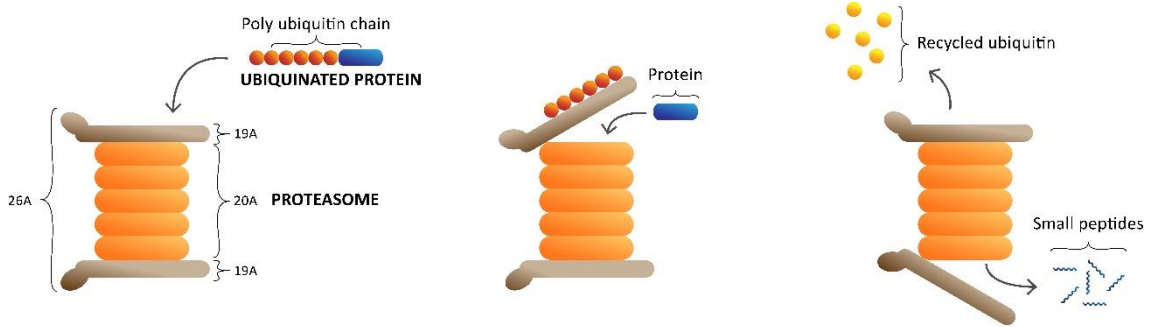
Figure 1.4 *Ubiquitin-proteasome system. Ubiquinated proteins reach the proteasome structure (left); proteasome activates and the protein enters the 20A* [14]

Controlling the type and the quantity of proteins present at any moment in the cytoplasm, the UPS can regulate fundamental cellular process, from cell cycle, metabolism, signal transduction to apoptosis, including mobility and growth. The disruption of the healthy balance of protein degradation is detrimental for the organism as it is connected to the development and the progression of a wide range of diseases including several cancers and, as a matter of fact, Multiple Myeloma [15]. The dysregulation of the UPS in MM results in the upregulation of the proteasome activity, manifesting itself in the excessive degradation of relevant substances such as the tumor suppressor p53 and IκB, the inhibitor of nuclear factor-κB (NF-κB) [13]. NF-κB is mainly implicated in the immune and inflammatory response, as it controls the expression of the signaling molecules involved, but its activation can additionally repress apoptotic signals, promoting the survival of MM cells and possibly resulting in drug resistance [14]. Proteasome dysfunction can therefore sustain oncogenic progression, providing signaling pathways that support the survival of the malignant cells and leading to rapid proliferation of MM cells in the bone marrow.

Proteasome inhibitors mechanism of action is against IκB degradation, inhibiting NF-κB transcription and sensitizing malignant cells to apoptosis. PI effectiveness in therapies resides in the fact that PCs and in particular the malignant ones are highly secretory cells, with a well-developed Endoplasmic Reticulum (ER), capable of huge synthesis of regular proteins and chaperone proteins in charge of proper Ig translation and folding [16]. For this reason, MM cells are more susceptible to the cytotoxic effects of PI, having an increased need for clearance of aberrant proteins, which otherwise accumulate in the ER, driving to ER stress and subsequently to the disruption of cell cycle regulation and to the activation of apoptotic pathways . [11], [14], [17].
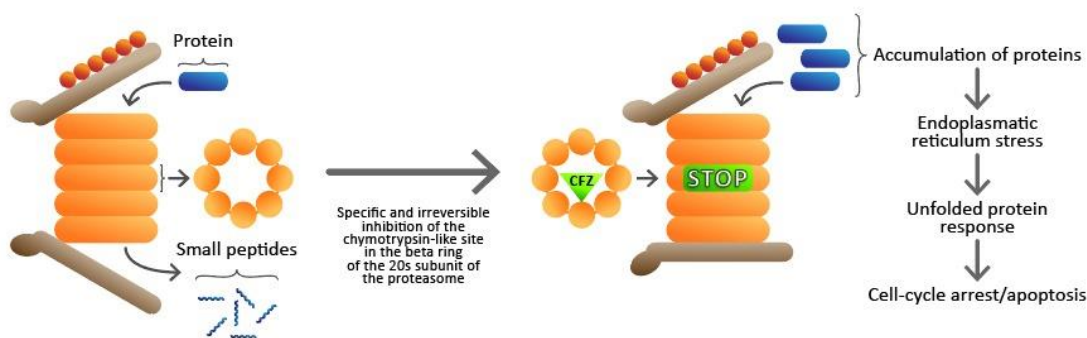
Figure 1.5 *CFZ, mechanism of action* [14].

AGI 6780: synergy with CFZ

In this project, one of the key ideas is to exploit the recently revealed efficacy of the combination if Carfilzomib with the IDH2 inhibitor AGI-6780 [18], [19]. As seen before, CFZ belongs to the second generation of PI; it is chemically a tetrapeptide epoxyketone (Figure 1.6Figure 1.6) and it was approved by FDA in 2012. Compared with BTZ, CFZ shows a better affinity to the proteasome, on which the CFZ molecule binds irreversibly, inhibiting proteasomal activity to less than 20% [16]. AGI-6780 instead acts on Isocitrate Dehydrogenase 2 (IDH2), a critical metabolic enzyme present in the mitochondria, implicated in the production of energy in form of ATP. IDH2 is in fact a NADP+-dependent homodimer, involved in the Krebs cycle, specifically in the catalysis of the oxidative decarboxylation of isocitrate (ICT), that generates α-ketoglutarate (α-KG), NADPH and CO_2 [20]. It has been

seen that in several malignancies IDH2 (together with IDH1, another IDH type, localized in the cytosol) is subjected to mutations which alter the epigenome, with pathogenic effects [21]. Mutant IDHs catalyze the reduction of α-KG (with oxidation of NADH into NADP+). The product of this reaction is an oncometabolite: (R)-2-hydroxyglutarate (R-2HG), which increases the multipotency the malignancy of tumor cells. In fact, the production of R-2HG inhibits α-KG-dependent dioxygenase function and lowers the levels of NADPH, necessary to activate various antioxidant substances, such as glutathione, the main responsible for preventing oxidative damage [21]. In this way, mitochondrial homeostasis and the redox state of the cell are altered: accumulation of ROS-species takes place, with consequent oxidative stress, lipid peroxidation and DNA damage [20].
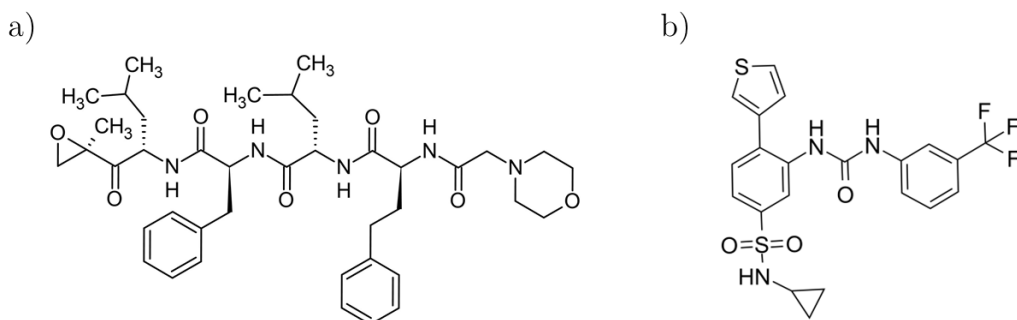
Figure 1.6 *Drug molecules: CFZ (a) and AGI-6780 (b)*

It has been recently proven that in MM, IDH2 inhibition enhances the effectiveness of proteasome inhibitors [18]. It was seen that the combination between AGI-6780 and PI, drastically decreases Krebs cycle activity, subsequently reducing ATP levels. This specifically happens due to the inhibition of the NF-κB/NAMPT/SIRT3/IDH2 pathway, that together with the inhibition of the proteasome activity, results in a synergistic enhanced cytotoxicity. This synergy represents thus a tool to better obstacle tumour progression and extend patient's survival, giving also the possibility to lower drug doses, diminishing systemic toxic effects [19]. One of the main ideas in this project is to exploit the lethal synergy, encapsulating AGI-6780 in silica nanoparticles because it is nearly impossible to administer due to its extremely high hydrophobicity and use the NP together with CFZ, that is currently administered in the therapy of patients with relapsed and refractory MM, being indicated for patients who underwent at least two previous therapies, including BTZ and IMiD [16].

9
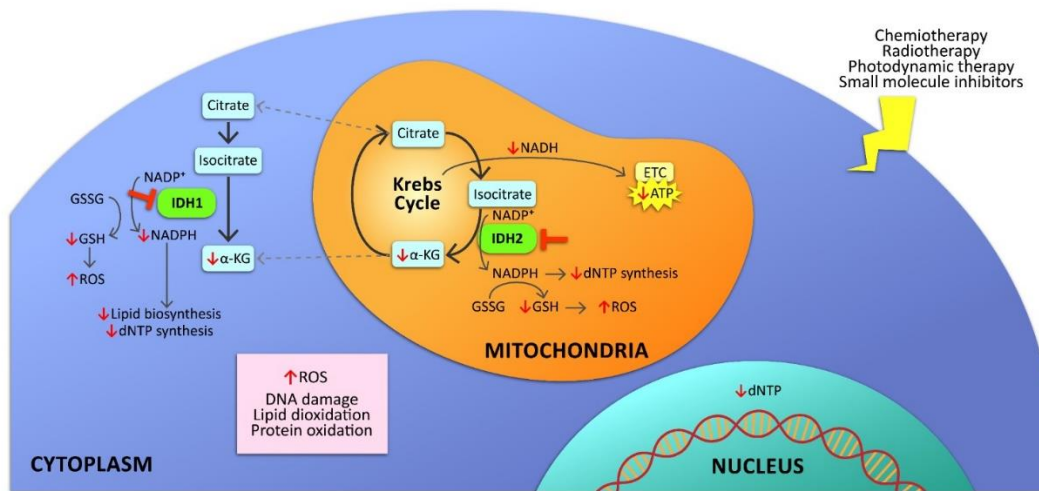
Figure 1.7 *IDH1/2 inhibition enhancing conventional cancer therapy efficacy. [19]*

1.2 Nanoparticles for drug delivery

Over the years, nanotechnology has evolved, becoming one of the key elements of scientific research in the current century. Nanotechnology is in fact an extremely versatile and transversal field, that has the potential to improve and revolutionize the development of every kind of technology and optimize aspects of any type of device. Particularly promising is the application of nanotechnology in the field of biomedicine; the introduction of nanomedicine (namely nano-formulated medicine) has in fact shifted the paradigms in therapies as well as in tissue engineering, providing extremely interesting materials, capable of interacting with the cells and the tissues at a molecular level. In this work the focus will be on nanoparticles, which have by now become a milestone in the development of new therapies and diagnosis methods. Recently it has been coined a new word:" Theranostic", which means that therapy and diagnostic are performed together, combining the ability to cure and image diseases (Figure 1.8). Nanoparticles are the perfect devices to fulfil this theranostic concept and over the years an impressive variety of NP has been developed and studied [22].
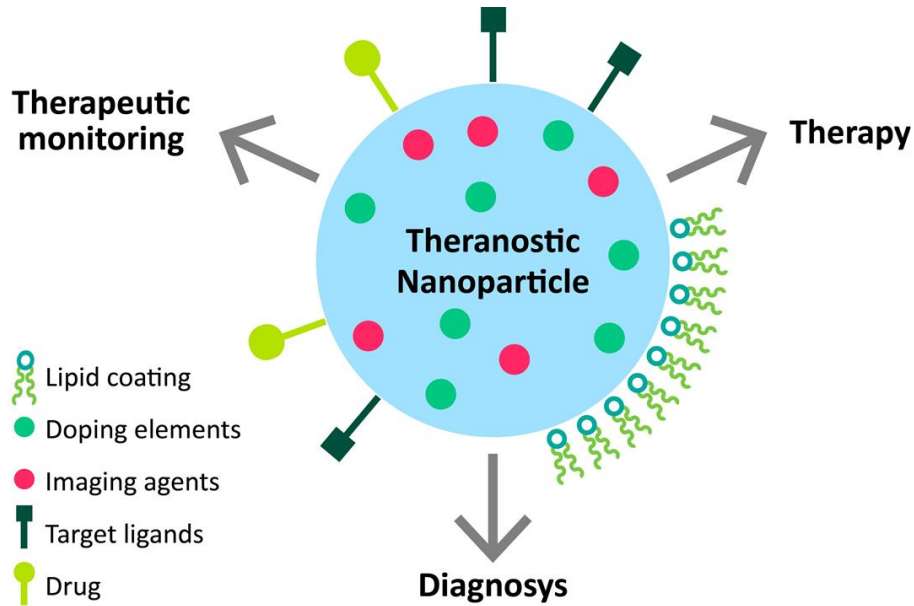
Figure 1.8 *scheme of a theranostic nanoparticle.*

Nanoparticles demonstrate a terrific potential as drug delivery systems and theranostic agents due to their many properties: NPs are characterized by a nanometric size, which implies an intrinsic great surface area to volume ratio, providing a wide surface for the therapeutic agents to be adsorbed. Moreover, their size allows an easy circulation in the blood stream and cellular internalization. NPs bring therapies, especially in oncology, a step forward, as nanocarriers give the possibility of a controlled drug release. Every drug has in fact a therapeutical window (Figure 1.99), in which the concentration of the drug in the organism is effective. Below the therapeutical window the drug is ineffective, due to its low concentration, above the upper limit the concentration of the drug is harmful or toxic for the organism. For this reason, an ideal administration should produce a constant concentration of the therapeutical agent in the fixed range. Conventional administration methods (oral, injection, inhalation, etc.) generate peaks and oscillations in the concentration of the drugs over time, which can easily drive the concentration out of the therapeutic window. The encapsulation of therapeutical agents in NPs, offers the possibility to a progressive and controlled release of the cargo, allowing a prolonged therapeutical effect [10],[22],[23].
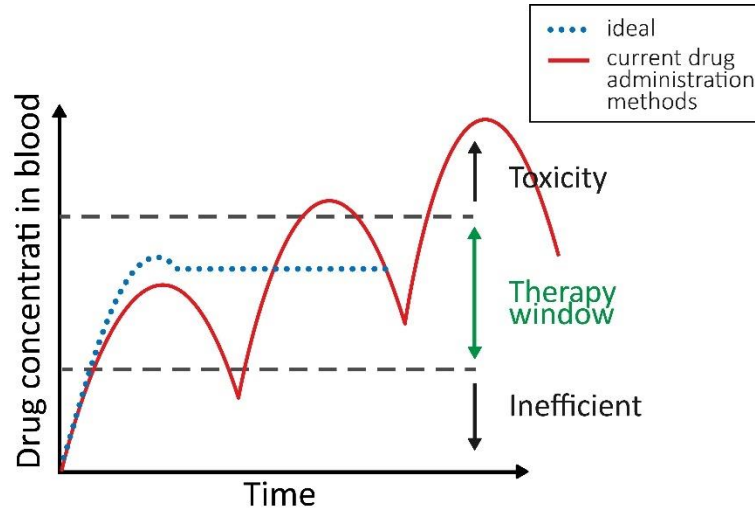
Figure 1.9 *Therapeutical window concept: the therapeutical agent should have a constant and controlled concentration in the organism to be effective against the battled pathology.*

NPs come also in a variety of morphology, chemical, magnetic and optical properties, that can be tuned and customized to better suit a specific medical purpose. NP have evolved over time from simple lipid-based nanocarriers (for example liposomes) becoming more and more complex systems. By now, NPs typically have a core, where normally is located the therapeutic agent, and a shell, an outer cap structure, which prevents the premature release of the cargo and is responsible for the biocompatibility of the whole NP. The core can be organic (e.g., polymer-based NPs), inorganic (quantum dots, golden or silver NPs, iron oxide NPs, silica NPs…) or even hybrid. The shell can be made by polymers or more complex biomimetic layers, such as lipidic bilayers that mimic cellular envelops. The surface compartment is responsible for making the NP "stealth", that means the NP can circulate unnoticed by the immune system in the blood stream, preventing in this way an inflammatory response. This is usually achieved with PEGylation (the coverage of the NP with PEG molecules avoids nonspecific adsorption of serum proteins, that triggers the immune response) or by covering the NP with biologically derived or synthetic biomimetic layers. Such shells can be also designed to be stimuli-responsive (e.g. temperature-, pH-, magnetic field-sensitive NPs), providing an environment-dependent or even an on-demand release of the cargo [22],[23].
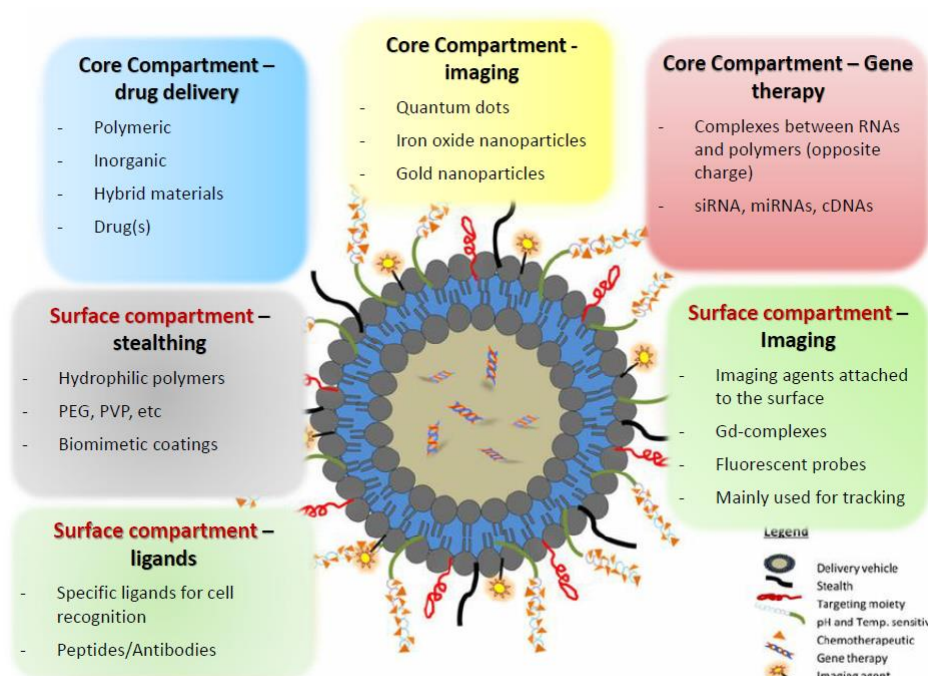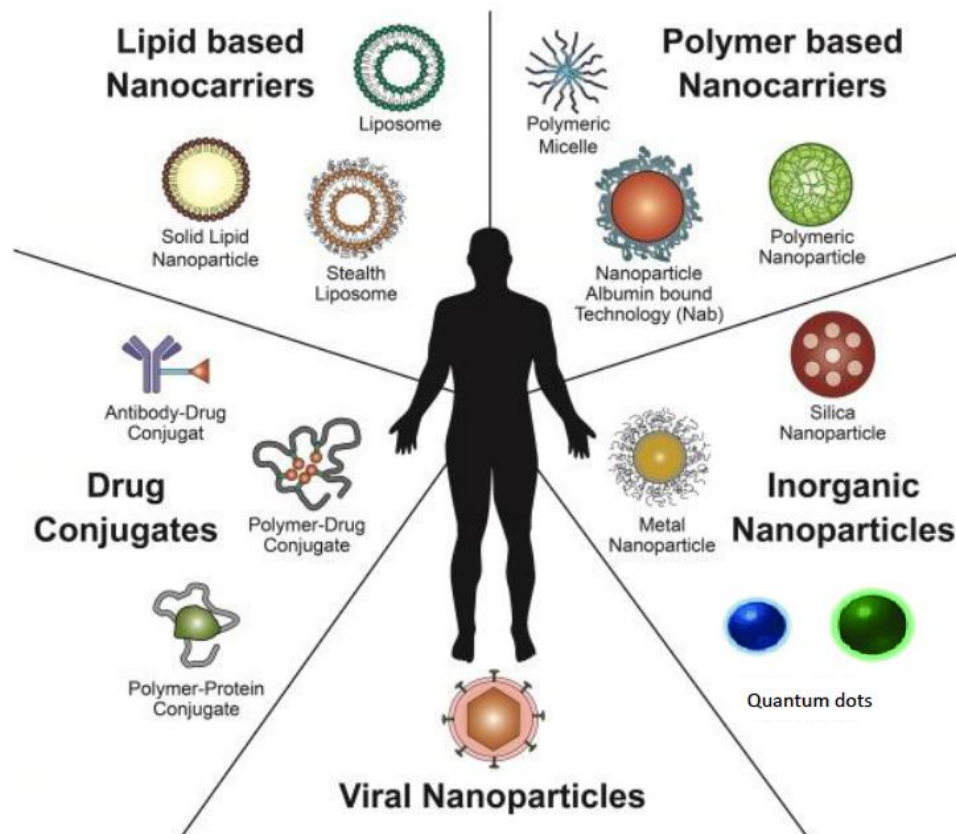
Figure 1.10 *Types and characteristics of nanoparticles.*

Passive targeting

The NPs described above have the potential to accumulate in the tumour micro-environment thanks to the Enhanced Permeation and Retention (EPR) effect. Several solid cancers are in fact characterized by a copious angiogenesis that gives birth to a structure of overabundant, disorganized blood vessels, meant to feed the malignant cells and support their uncontrolled growth. The endothelium of the cancer vessels results defective and commonly presents fenestrations (up to 4 μm) through which macromolecules (>40 kDa) and small sized NPs (from 10 to 400 nm) can reach and accumulate in the surroundings of cancer cells thanks to extravasation through the leaky vessels [10]. This is called passive targeting, and the efficacy of therapies relies on the small size of the NPs and to the lack of efficient lymphatic drainage typical of the tumoral environment. Unfortunately, not every type of cancer (particularly large tumours) shows EPR phenomenon and if it is present, NPs often fail to reach malignant cells due to adverse pressure gradients that take place in the surroundings of the cancer. NPs that rely on passive targeting are also subjected to clearance by mononuclear phagocytic system and accumulation in sites different from the target tissue, such as liver and spleen [10].

Active targeting

What may overcome the limitation of passive targeting is the active targeting, which consists in the functionalization of the external surface of the NPs with targeting moieties (i.e. antibodies, aptamers, peptides, other biological or synthetic ligands) that specifically interact with receptors uniquely present or overexpressed on the membrane of malignant cells. Ligand-based targeting allows preferential accumulation of NPs in the tumoral environment, restricting the therapeutic effect to cancer cells, thus reducing systemic toxicity and avoiding side-effects. Moreover, ligand-receptor interaction can trigger receptor-mediated endocytosis, facilitating NP internalization. It additionally opens the possibility to address not only solid tumour, as in the case of passive targeting, but also to target circulating cancer cells in hematological malignancies. For the reported reasons, the active targeting approach has the potential to increase overall drug safety, ensuring appropriate NP concentration in the targeted site and consequently increasing the therapeutic index (maximum tolerated vs minimum effective drug dose ratio) [10],[24],[25].

MSN: Mesoporous Silica Nanoparticles

Nanostructured materials are defined as materials having in their structural elements a nano-sized component, namely in the range between 1 and 100 nm [26]. Mesoporous materials belong to the nanostructured materials and are defined, according to IUPAC classification, as porous materials characterized by an ordered structure of nanopores, ranging in dimension between 2 and 50 nm. The other 2 categories of nanostructured materials are microporous materials, with porosity in the range of 50-100 nm and microporous ones, with pore dimensions inferior to 2 nm.
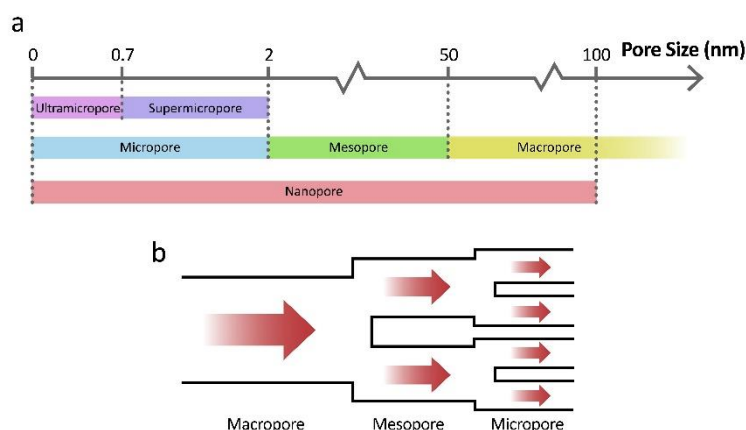
Figure 1.11 IUPAC *classification for nanoporous materials: macropore* → *pore diameter = 50-100 nm; mesopore* → *pore diameter = 2-50 nm; micropore* → *pore diameter < 2 nm.*

Mesoporous silica is the mesoporous and amorphous form of silicon dioxide. In the last years, Mesoporous Silica Nanoparticles (MSNs), have gained immense attention and thanks to their enormous versatility and their unique properties, (first of all their great surface-to-volume ratio) have reached success in various application areas, such as catalysis, sorption, chromatography, water purification and the development of systems capable of controlled release of active compounds [27]. In particular, MSNs have been promoted in biological and medical research, becoming one of the most well-established inorganic material to convey a wide variety of therapeutic agents, expecially chemotherapics [22], [28]. Their specific surface of approximately 1000 m²/g and their pore volume (about 1 cm³/g) makes in fact MSNs an ideal substrate to prepare nanocarriers with great cargo loading capacity,

delivering all sort of molecules (drugs, macromolecules, proteins, siRNA, and so forth). They also show colloidal stability and uniform pore diameter (in the range from 2 to s50 nm), thus providing accessible nanoscale morphologies [29]. MSNs are characterized by intrinsically wide and easily functionalizing surface and tunable physical properties: the external shape and morphology of the NP (spherical, rod-like...), the pore dimensions, volume and shape can be easily tuned controlling the synthesis parameters. MSNs are also relatively simple to produce and cost effective; moreover, their surface chemistry can be easily functionalized. Since MSNs can be customized to better accommodate the cargo molecules, they have the potential to become part of effective and versatile therapeutic, diagnostic and theranostic platforms [22],[23],[29]. MSNs in vivo safety and biocompatibility has been widely studied and proven; MSNs were found to be safe and well tolerated by the organism if administered orally or by intravenous injection [22],[30],[31].

MSNs synthesis

There are different methods to synthetize MSNs, resulting in an incredible diversity of engineered particles. The first reported mesoscopic solid material was synthetized with the liquid crystal template mechanism in 1992 by Mobil Research and Development Corporation. MSNs were produced from aluminosilicate gel together with cationic surfactants as templates, obtaining what was called MCM-41 (Mobil Crystalline Materials). MCM-41 is one of the most exploited and studied materials for nanocarriers development; it is characterized by hexagonal structure, with a pore diameter ranging from 2,5 to 6 nm. Modifying the starting precursors and acting on the condition during the reaction, also MCM-48 and MCM-50 were developed. Similarly, also in University of California, Santa Barbara, were first synthetized various forms of mesoporous silica structures: the Santa Barbara Amorphous type materials (SBA). SBA were produced using as surfactants non-ionic triblock copolymers (e.g. PEO) and poly(alkylene oxide) block copolymers as templates. These experimentations gave birth to SBA-11, SBA-12, SBA-15 and SBA-16, whose structural properties are listed in Table 1.2, together with other famous MSN formulations developed over the years in other laboratories [22]. To be mentioned, thanks to its great potential, is a novel type of MSNs: Hollow mesoporous silica nanoparticles (HMSNs). As the name suggest, HMSN are MSN with a hollow cavity, that allows the storage of much higher amounts of drug, if compared to the non-hollow counterparts [22].

Table 1.2 *MSNs types and relative characteristics.*

MSN Family	MSN Type	Pore Symmetry	Pore Size (nm)	Pore Volume (cm³/g)	Particularly employed in:
M41S	MCM-41	2D hexagonal *P6mm*	1.5-8	>1.0	Drug delivery
	MCM-48	3D cubic *Ia3d*	2-5	>1.0	Drug delivery
	MCM-50	Lamellar *p2*	2-5	>1.0	Catalysis and absorption
SBA	SBA-11	3D cubic *Pm3m*	2.1-3.6	0.68	Catalysis and absorption
	SBA-12	3D hexagonal *P63/mmc*	3.1	0.83	Catalysis and absorption
	SBA-15	Cubic *Im3m*	6-10	1.17	Drug delivery
	SBA-16	2D hexagonal *p6mm*	5-15	0.91	Drug delivery
KIT	KIT-5	Cubic *Fm3m*	9.3	0.45	Catalysis and absorption
COK	COK-12	Hexagonal *P6m*	5.8	0.45	Catalysis and absorption
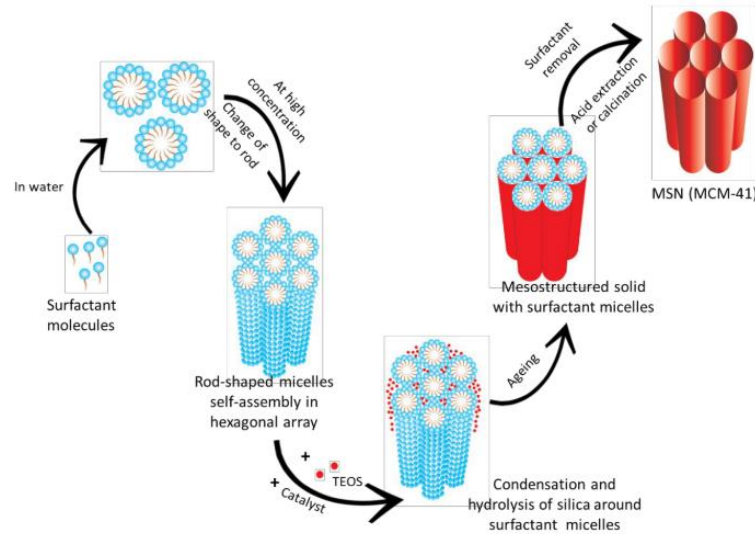
Figure 2. Mechanism of formation of Mobil Crystalline Materials No.41 (MCM-41).

Figure 1.12 *Synthesis mechanism of Mobil Crystalline Materials 41 (MCM-41) [22].*

For what concerns the synthesis mechanism, the Stöber's method, also known as sol-gel process, has been the starting point for the development of many synthesis methods, pioneering the development of stable, monodisperse, ordered and spherical MSNs [22]. Basically, in Stöber's synthesis, alkoxide monomers, that are liquid silica precursor (e.g. tetraethyl orthosilicate, TEOS) are subjected to hydrolysis and form

a colloidal solution (sol). Subsequently, condensation takes place, forming a 3D amorphous silica network (gel) around surfactant micelles, which self-assemble in an ordered configuration that serves as template for the pores. By removing the surfactant template (through calcination or acid extraction) the mesoporous structure is achieved. By changing the parameters (type and concentration of the surfactant, temperature, pH, the reaction mixture, etc.) different silica structures, pore volumes and NP shape are obtained [22].

Supported Lipid bilayers (SLB) and Protocells

A novel approach, that is the one followed in this Master Thesis, is to coat MSN with lipid bilayers, mimicking natural cellular envelops. NPs produced in this way are called "protocells" and combine the advantages of MSNs: porous and ordered structure, great loading capacity, tuneable size and shape, and advantages of the liposomes: increased circulation time, low toxicity, higher hemocompatibility, easy surface modification to include functional groups and consequently the possibility to be easily internalized by cells. Lipid Bilayers (LB) coating enhances the biocompatibility and improves the pharmacokinetics of the MSNs, preventing them to aggregate and providing a cap system that entraps the drug in the silica pores, avoiding cargo release before cell internalization of the NPs. Moreover, as anticipated, LB allows the NPs to be easily functionalized for active targeting; with LB coating this can be done independently from MSNs surface properties [32].
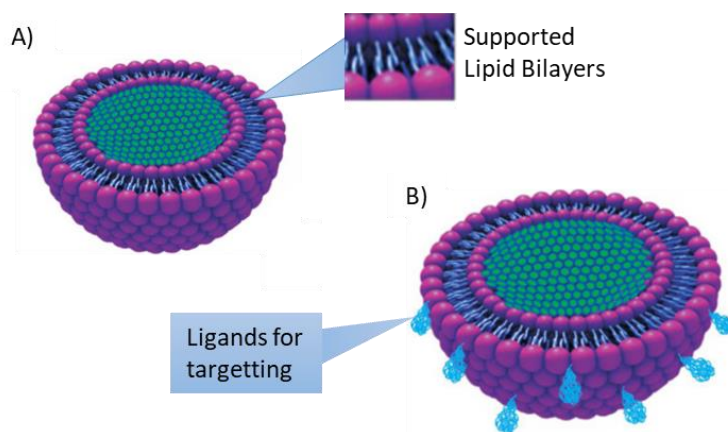
Figure 1.13 *Representation of (A) Non-targeted and (B) targeted protocell.* [22]

18

1.3 Selective targeting and Functionalization against MM

As previously discussed, active targeting, with functionalization of the outer part of the nanoparticles with specific ligands is essential to efficaciously address cancer cells, exploiting the presence of characteristic receptors on malignant cell microenvironment. Immunotherapy strategy shares with NP-active targeting the same selective binding principle; yet in the case of immunotherapy the focus is on exploiting receptor specificity to stimulate host response or induce malignant cell death through the activation of receptor-mediated apoptotic pathways [25],[33]. In both cases, the deep understanding of cancer cell characteristics and above all the identification of specific antigens, together with their binding mechanisms and downstream effects, is fundamental to develop such strategies. By now, CD38 has been elected as the most interesting target antigen in MM cells, as it is highly expressed in their membrane [34]. Nonetheless, other surface molecules have been explored as potential targets, e.g. CD138 which, despite being the major marker to detect MM cells, is affected by drug exposure and hypoxia, and VLA-4 marker, which is expressed in several malignancies and its exposure on MM cells is very heterogenous [10] [34].

Specifically, CD38 antigen in humans is a type II transmembrane glycoprotein, associated with several pathologies such as HIV, autoimmune diseases, osteoporosis and cancer, particularly in hematological malignancies. Among them, expression of CD38 was especially seen in MM [34]. It has been observed that CD38 not only fulfils receptor tasks, but is a pleiotropic molecule with multiple functions, that include ecto-enzymatic activity, being involved in the production of cyclic ADP-ribose and ADPR (cyclase and hydrolase action) [33],[34].

Immunoglobulins and immunotherapy

Antibodies (Abs) or immunoglobulins (Ig) are complex glycoproteins (approximately 150 kDa) produced by PCs, with fundamental role in host defense, being responsible of opsonization and recruiting effectors of the immune system. They are the result of 400 million years of evolution and have gained superb functional properties i.e. extreme specificity and affinity towards their respective antigens, and a long serum half-life. Thanks to their excellent and precise target selectivity, that

means lower toxicity, monoclonal antibodies (mAbs) have achieved a leading role in pharmaceutical industry, substituting small molecules. As a matter of fact, with monoclonal antibodies introduction, MM treatment underwent important changes and the possibility to cure patients with immunotherapeutic strategies was established [34],[35].

Antibodies have a characteristic "Y" shape, composed by a complex quaternary structure that results from the folding of unique tertiary domains (Figure 1.14 *(A) Monoclonal antibody structure, with light (L) and heavy (H) chains, connected through inter-chain disulphide bonds. Light and heavy are composed by constant (C_L, C_H) and variable (V_L, V_H) domains.* **(B) Denomination of antibodies depending on the amount of human sequences present. Immunogenic potential decreases increasing the number of human domains.** [35]. In fact, although the diverse types of Ig share a common overall structure having same constant domains (C), every Ig shows particular variable domains (V), which selectively interact with their specific antigen. Until now, five classes of antibody have been discovered: IgA, IgD, IgE, IgM, and IgG. IgG represent approximately the 80% of the antibodies present in human serum and are the most approved antibodies in therapeutics. Ig are composed by four polypeptide chains: 2 heavy (approximately 50kDa) and 2 light chains (25kDa ca.), held together with disulphide bonds. Heavy chains comprise 3 constant domains (C_H1, C_H2 and C_H3) and a variable domain (V_H) whereas light chains are composed by a variable domain (V_L) and a constant domain (C_L). Another distinction in the Ig structure can be done between different fragments, that can be obtained through reduction or proteolytic digestion of the antibody by enzymes i.e. pepsin and papain. Papain divides Igs in 3 fragments: two identical branches, Antigen Binding Fragments (Fabs) consisting of a light chain with the upper part of the heavy chain, and the remaining stem segment, the Crystallizable Fragment (Fc), composed by the bottom part of the heavy chains. Fabs can be further divided into Fv, which consists of the variable domains uniquely. On the other hand, pepsin digestion occurs with the elimination of the bottom part of the heavy chains (C_H2 and C_H3), generating a single fragment, $F(ab')_2$, [35].
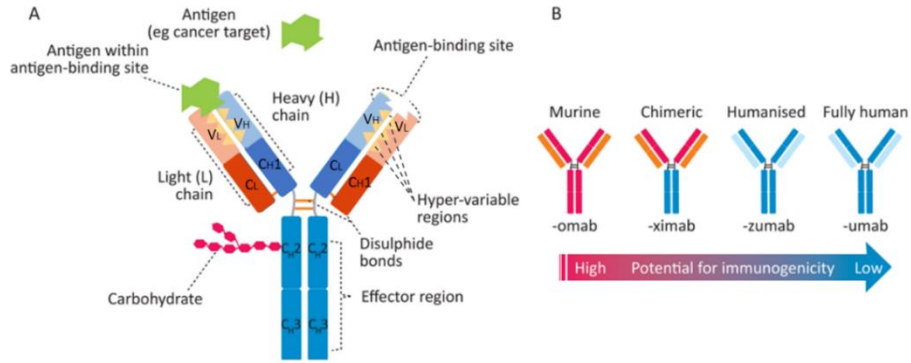
Figure 1.14 *(A) Monoclonal antibody structure, with light (L) and heavy (H) chains, connected through inter-chain disulphide bonds. Light and heavy are composed by constant (C_L, C_H) and variable (V_L, V_H) domains. (B) Denomination of antibodies depending on the amount of human sequences present. Immunogenic potential decreases increasing the number of human domains. [35]*
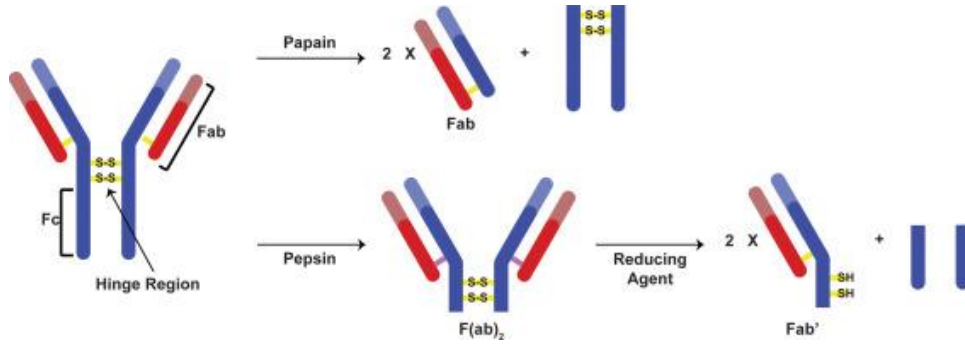
Figure 1.15 *Antibody reduction with Papain or Pepsin and consequent generation of antibody fragments Fab, F(ab')2 or Fab'.*

Several monoclonal antibodies are employed in Immunotherapy and the cytotoxic effect is reached exploiting the natural ability of mAb to stimulate immune defense mechanism against cancer cells. Tumor cells death can be induced by various mechanisms: ADCC (antibody-dependent cellular cytotoxicity), ADCP (antibody-dependent cellular phagocytosis) and CDC (complement-dependent cytotoxicity), where Igs trigger the response of immune effectors (mainly Natural Killers), monocytes and macrophages, and complement cascade respectively [33], [35]. Many mAb exert their action with ulterior mechanisms: directed against tumor receptors, they interfere with the function of the addressed proteins, blocking signaling activity of growth factor receptors or causing the disruption of cellular pathways, leading eventually to apoptosis [25],[36].

Anti-CD38 monoclonal antibodies

Thanks to its high level of expression and its role in cell signaling, CD38 is very appealing as therapeutic antibody target. Various promising anti-CD38 agents were developed, first of all Daratumumab, also referred to as HuMax-CD38 and IgG1-005, which has already been FDA approved and designated for the treatment of MM patients after the third line of therapy. Daratumumab (DARA) is a human immunoglobulin G1 kappa (IgG1k), which specifically and strongly binds to a CD38 epitope, efficiently mediating CDC mechanism. Other CD38-targeting antibodies (e.g. isatuximab AND Takeda's Ab79 and Ab19) were developed, showing strong preclinical and clinical potential [33], [34].

An interesting aspect of mAb employment in oncologic treatments not yet discussed is that their mechanism of cytotoxicity differs significantly from existing therapies, such as IMiDs and proteasome inhibitors. This means that mAb therapy can be conveniently combined with other therapeutical agents, gaining all the advantages of the synergistic action (i.e. enhanced efficacy, lower drug dosages and reduced toxicity) [34], [36], [37].
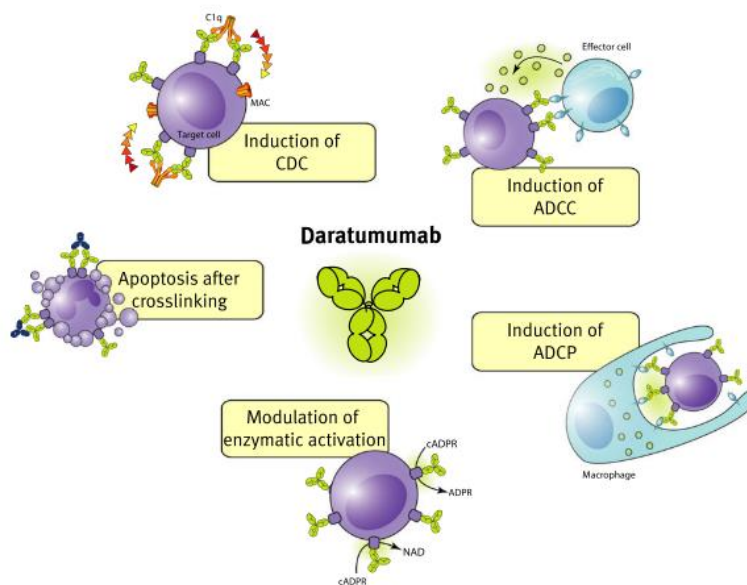
Figure 1.16 *Mechanism of action of Daratumumab* [34]**.**

22

2 Materials and methods

2.1 Synthesis and characterization

Synthesis of aminopropyl-functionalized MSNs

MSNs were obtained performing a Stöber's synthesis known also as template-assisted sol-gel self-assembly process. The used silica precursor is TEOS (tetraethyl orthosilicate, 98%, Sigma-Aldrich). The process consists in hydrolyzing and condensing a silica precursor around a self-assembled micellar structure of a cationic surfactant, in this case CTAC (cetyltrimethylammonium chloride, Sigma-Aldrich). In this way the silica structure hydrolyses and condenses on the template formed by the organic surfactant (liquid crystals), providing the characteristic ordered mesoporous architecture.
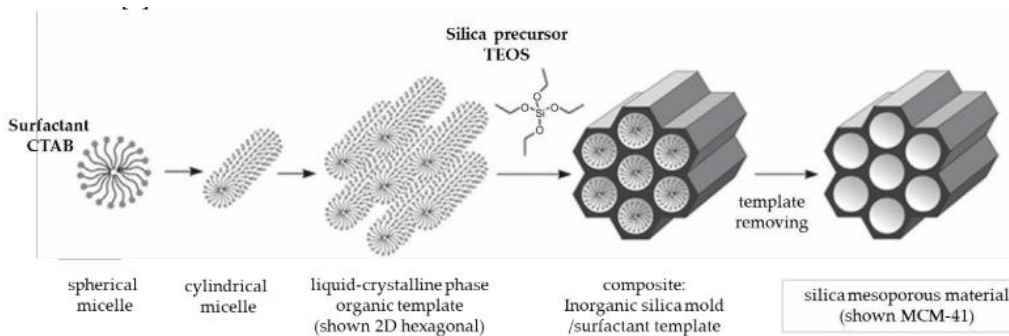
Figure 2.1 *MSNs synthesis: Stöber's process* [27].

To perform the Stöber's process, a mixture of 2.41 mL of CTAC and 21.7 mL bidistilled water (from a milli-Q system, Millipore) was prepared and heated up to 60 °C. A second solution was obtained mixing 19.2 g TEOS and 14.3 g TEA (triethanolamine, 99%, Sigma-Aldrich) and heating in a 100 mL polypropylene reactor without stirring at 90°C for 20 minutes. Successively, the two solutions were rapidly combined and homogenized by stirring for 30 min at 500 rpm (VELP Scientifica, AREX DIGITAL).

To obtain the functionalization of the external surface of the MSNs with aminopropyl groups (-NH$_2$), exactly after 30 min stirring of the above-described solutions, a third solution was added. This last mixture consists of 20.6 µL TEOS (which corresponds to 1 molar% of the first TEOS solution) together with 16.1 µL

23

APTES (3-aminopropyltrimethoxysilane, 98%, Aldrich). Then, the solution was stirred overnight at room temperature (RT) at 500 rpm. The following day the obtained mixture was washed adding 100 mL of ethanol (EtOH, 96%, Sigma-Aldrich), to promote flocculation and NPs deposition. Successively, the solution was divided between two 50 mL Falcons and centrifuged (VWR, Mega Star 600R) for 10 min at 10˙000 RCF (Relative Centrifugal Force). The supernatant was then removed.

Liquid crystal template removal

To extract the liquid crystals template from the silica structure, the pellet was resuspended in 100 ml of a solution consisting of 2 g ammonium nitrate (NH_4NO_3, 98%, Sigma-Aldrich) in 100 mL EtOH, and stirred in a multi-neck round bottom flask, partially immersed in a preheated 90°C silicon oil bath, for 45 min at 350 rpm under reflux conditions.

The nanoparticle suspension was then centrifuged for 5 min at 10˙000 RCF, the supernatant was discarded, and the MSNs resuspended in a second solution of 10 vol% of HCL (37%) in 100 mL EtOH. Again, the MSN underwent to reflux conditions for 45 min in the round bottom flask. Finally, the MSNs were washed three times in EtOH followed to centrifugation (10˙000 RCF, 5 min). Finally, the pelleted MSNs were resuspended in 15 mL EtOH and stored at room temperature.

To measure the final concentration, 1 mL of the NP colloidal suspension was collected and dried in oven at 60°C. When the complete evaporation of EtOH was reached, the dried NP were weighted trough a precision scale.

FE-SEM - *Field Emission Scanning Electron Microscopy*

Field Emission Scanning Electron Microscope (FE-SEM) is an instrument used to obtain highly magnified and greatly resolved images of superficial micro- and even nano- structures. This technique, as all the Scanning Electron Microscopies (SEM), employs an accelerated electron beam, that is focused on the sample surface through electromagnetic lenses. Electron microscopy allows much superior resolution compared to optical microscopy, since electrons possess shorter wavelength

than photons. In fact, according to Abbe's equation, resolution is directly proportional to wavelength of the radiation beam.

$$d = 1.22 \ \frac{\lambda_{vac}}{n \cdot sin\theta} \tag{1}$$

Where d is the resolution, λ_{vac} the wavelength of the radiation in the vacuum, and $n \cdot sin\theta$ the numerical aperture. What mainly differentiates SEM from FE-SEM is the production of the electron beam: in SEM the primary electron beam is obtained through thermionic emission of a heated tungsten filament, placed into a powerful electric field, which accelerates and directs the particles towards the specimen. In FE-SEM, an extremely sharp tip (apical radius in the order of 100 nm) of a high melting point metal (typically tungsten) is placed in a high electric field. Thanks to the size and the shape of the metallic tip, it is possible to produce a neater, more focused electron beam with lower voltages than SEM. This allows the production of clearer and better resolved images.

In both technologies, ultrahigh vacuum is needed to minimize interaction between beam and air, permitting the electrons to directly reach specimen. Here, the electrons hit the surface of the sample and can be adsorbed, reflected of transmitted. For surface topography reconstruction, the electrons of interest are the secondary electrons (SEs), i.e., electrons of the specimen that are ejected when hit by the beam. In particular, slow SEs (with energy < 50 eV) are detected and used to generate the image. In fact, since they are very weak, they can only escape if they come from near the specimen surface.

In Scanning Electron Microscopes (SEM), the primary electron emission is achieved by thermionic emission from a tungsten filament, which is put into a polarizing field and heated through Joule effect until electrons are free to escape from the metal and can be accelerated toward the sample. FESEM uses a different approach to generate the electron beam: a sharp tip of tungsten is put in a high electric field, and thanks to its shape and small size electrons are generated at lower voltages, producing clearer images with an improved spatial resolution. When the sample is hit, secondary electrons are emitted from each spot and collected by a detector, and their angle and velocity depend on the surface structure of the object. The detector produces an electric signal, which is amplified and transformed into an image.

In this work, a Carl Zeiss Merlin FE-SEM was employed. The samples were prepared by dropping on a silicon wafer a 100 µg/mL ethanol solution of MSNs. [38], [39].

Nitrogen absorption (BET)

To characterize the porosity on the MSNs, in terms of specific surface, pore size distribution, cumulative volume and pore morphology, gas adsorption analyser (ASAP 2020Plus version 2, Physisorption, Micrometics) was used. The instrument relies on nitrogen physisorption phenomena on the eternal surface and in the pores of mesoporous silica. Physisorption, differently from chemisorption which happens through a primary chemical bond between a surface and the adsorbed gas, consists in weak bonds and Van der Waals interaction between gas and surface. It is a reversible phenomenon and it is impaired by high temperatures, which weaken surface-gas interactions. It is instead promoted by pressure increase. For that reason, the instrument works at a constant temperature of 77K (-196°C) and adsorption-desorption isotherms are obtained measuring the quantity of adsorbed and then desorbed gas (nitrogen) as a function of the applied pressure. Before the real measurement of isotherms, some preliminary operations are needed:

- Pre-degassing operations: approximately 30 mg MSNs were completely dried in oven at 60°C. A void quartz glass burette with its inner bar and relative cap and O-ring was weighted as tare. A quantity in the range between 5 and 10 mg of dried MSNs was inserted in the burette and the gross was weighted.
- Degassing, that consists in heating the sample, and contextually reducing the pressure beyond 10 µmHg. this is necessary to remove humidity and to clean the sample from impurities and other adsorbed species. The imposed degassing condition were: hold temperature = 120°C (a relatively low temperature was chosen in this case, to avoid damage of the functional groups present on MSNs surface); hold time = 300 min (a long time to compensate the low hold temperature); target = 30°C. During degassing protocol, also free space (or dead volume) is measured employing helium, which is non-adsorbing. At the end of the process, the instrument

autonomously performs the backfill, i.e., fills the burette with a small amount of nitrogen, generating a little overpressure.
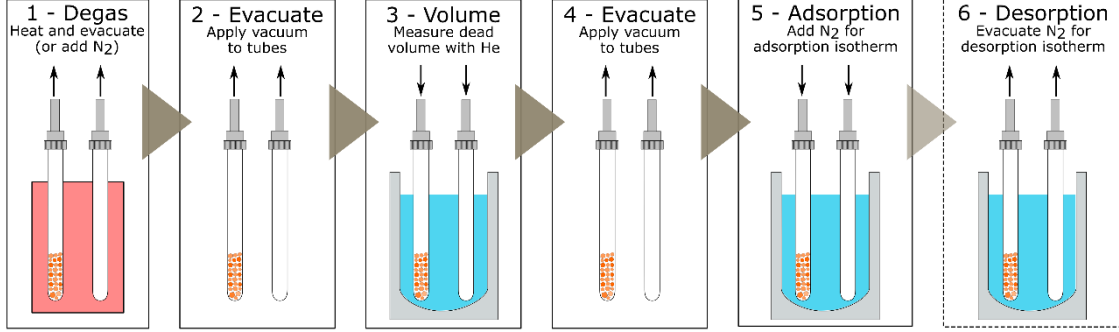
Figure 2.2 *Steps in nitrogen adsorption-desorption measurement* [40].

After degassing, the burette with the sample was again weighted and, after setting analysis conditions (silica alumina nitrogen @ 77,35 protocol) the measurement was started. From adsorption-desorption isotherms, data relative to the type of porosity of the material can be extracted, applying mathematical models: through BET (Brauer-Emmett-Teller) theory it is possible to calculate the total surface area and with DFT (Density Functional Model) pore size and distribution are estimated. BET isotherm model is an evolution of Langmuir isotherm, since it contemplates the formation of multilayers of adsorbate. The expression to calculate the volume of a monolayer (v_M) is:

$$\frac{p}{v_{ads}\,(p_0 - p)} = \frac{1}{v_M C} + \frac{C-1}{v_M C}\left(\frac{p}{p_0}\right) \qquad (2)$$

Where v_{ads} is the adsorbed volume at pressure p, p_0 is the adsorbate saturation pressure (p/p_0 is the relative pressure) and C is an empirical constant. Since v_{ads} is defined as the amount of adsorbent sufficient to generate a molecular monolayer that covers all the surface, from its value it is possible to obtain an evaluation of the specific surface.

Fourier-transform infrared spectroscopy FTIR

Spectroscopy is a set of techniques based on the relation between matter and electromagnetic waves (EM waves). What is measured is in fact the spectra of interaction between matter and EM radiation and the eventual presence of resonance peaks, which can be caused by emission, absorbance or scattering of the EM waves. In the case of infrared spectroscopy, the radiation corresponds to the emission of photons in the IR frequency range. Here the radiation is characterized by wavelengths between 0.7 and 3 μm, able to excite the molecular bonds, triggering their vibration. When excitation of interatomic bonds happens, the IR photons are adsorbed. The aim of FTIR technology is to understand which frequencies are most adsorbed, because every type of bond is characterized by its own vibration frequency and generates typical peaks in the spectrum. In this way information about the chemical nature of the specimen can be extracted. The sample is placed between the source of IR radiation and the detector, that collects the transmitted radiation, i.e., the part of the radiation that was not absorbed (transmission and absorption are complementary). In FTIR, data are recorded in time domain and then transformed into frequency domain generating the absorption spectrum in the infrared region. Infrared spectrum can be divided into two regions: the functional group region (frequencies from 4000 to 1000 cm^{-1}), which gives information about the type of bond present in organic molecules, such as functional groups, and the fingerprint region (frequencies below 1000 cm^{-1}), where the spectra produced are characteristic of large molecular fragments or even an entire molecule. Fingerprint region is thus used for molecular identification [38].

For the measurement, a sample of 500 μg in ethanol of MSNs was prepared and pipetted a single drop at a time (next drop was pipetted after the previous one was dried) onto a fragment of silica wafer (2x2 cm approximately). A naked silica wafer was prepared to obtain a background spectrum, that is automatically removed by the instrument from the spectrum of the sample.

The instrument used is a NICOLET 5700 FTIR spectrometer and the set parameters were: number of scans = 64, resolution =2 cm^{-1}, the automatic atmospheric suppression was activated, and absorbance was chosen as final format.

Dynamic Light Scattering DLS

Zetasizer Nano ZS90 (Malvern Instruments, Worcestershire, UK) was used to identify the Hydrodynamic Radius (R_H) of the MSNs. The R_H of a particle in a solvent is defined as the radius of a solid sphere that diffuses with the same speed as the measured particle. In other words, particles or macromolecules diffuse in a solvent following random Brownian motions; the smaller is the particle, the faster are the movements. The R_H takes account not only for the dimensions of the particle itself, but also for the ions and the proteins the surface may attract, which form a sort of coating around the particle and move with it. Therefore, R_H depends on shape, superficial properties and ionic strength of the particle. In DLS technology, a monochromatic light beam hits the sample (particles dispersed in a particular solvent, normally water); part of it passes unaltered, the other part scatters and is collected by a detector. Depending on the diffusion rate of the particles, which in turn depends on their size, the intensity of the scattered light that reaches the detector fluctuates with minor (big particles) or greater (smaller particles) frequencies.

To measure the R_H a further step is done: the first signal originated from detector (corresponding to time zero) is compared through correlation function with the signals of each following time point. The correlation is a measure of the similarity between 2 signals; if signals stay similar for a long time (and so correlation remains high), the sample is composed by large particles, which produce slow fluctuations in the output signal. On the other hand, if the correlation function decays rapidly, it is indicative of small particles, which generate faster fluctuations in intensity. Numerically, the R_H is calculated by Stokes-Einstein equation:

$$R_H = \frac{(k_B T)}{6\pi\eta D_t} \qquad (3)$$

Where k_B is Boltzmann's constant, T is the temperature and η is the viscosity of the dispersant; D_t is the diffusion time, extracted from the correlation function.

Measurements were performed for uncoated and lipid-coated MSNs, the latest were evaluated both pre- and post-dialysis. The samples were prepared in ethanol (only uncovered MSNs) or in Milli-Q bidistilled water (both uncovered and lipid-

coupled MSNs) with concentration of 400 µg/mL. 1 ml of sample was inserted in a 1ml cuvette (DTS0012 cuvette) immediately after its preparation and the measurement was started. For each sample 3 measurements were taken and then averaged.

Zeta potential

The same instrument: Zetasizer Nano ZS90 (Malvern Instruments, Worcestershire, UK); and the same samples: uncoated and lipid-coated MSNs, pre- and post-dialysis as DLS have been employed to evaluate the ζ potential of the nanoconstructs. When a material (MSNs in this case) gets in touch with a liquid, the formation of a surrounding double electronic layer occurs, depending on the electrical characteristics of its surface. Specific superficial charge of the MSN attracts counterions from the dispersant, which form a first, stable electrical layer around the particle, called Stern layer or stationary layer. In the surrounding of this first Stern layer, an outer electrical layer forms; it is characterized by weaker cohesion and interaction between charges, being more distant from the solid particle. The outer layer is thus able to move and for that reason it is called diffusion layer and the plane between the inner and outer electrical layers is named slipping or shear plane. ζ potential is defined as the potential that is generated between the Stern and the diffuse layer i.e., the potential measurable upon the slipping plane.
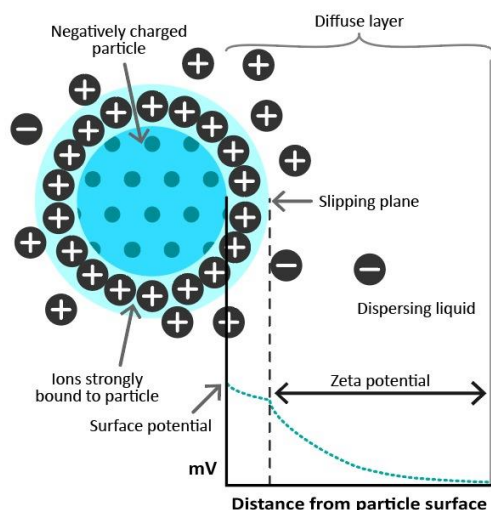
Figure 2.3 *Scheme of a particle immersed in a liquid dispersant: formation of Stern (inner) layer and diffuse (outer) layer and their relative zeta potential.*

More in detail, ζ potential is measured through an electrophoresis test: the samples are loaded in a special cuvette (DTS1070 capillary cuvette), which possess two electrodes. It is thus produced an electric field in which the NP are immersed and move faster or slower attracted by one of the two electrodes. The electrophoretic mobility (U_E), namely the ratio between the velocity v of the particles and the applied field strength E can be calculated through Henry's equation:

$$U_E = \frac{v}{E} = \frac{2\varepsilon\zeta F\ ka}{3\eta} \qquad (4)$$

Where ε and η are respectively the dielectric constant and the viscosity of the dispersant and $F\ ka$ is Henry's function, dependent on the thickness of the electrical double layer k and the particles radius a. The speed of the particles is evaluated thanks to Doppler effect of the scattering light using the following equation:

$$\Delta f = \frac{2v\,sin\left(\frac{\theta}{2}\right)}{\lambda} \qquad (5)$$

Δf is the frequency shift of the scattered light, θ the scattering angle and λ the laser wavelength. The samples are the ones dispersed in water, used previously for the DLS analysis. Measurements were taken 3 times per sample an than the mean was calculated and plotted.

Nanoparticle Tracking Analysis (NTA)

Coated MSNs size distribution was measured also using Nanoparticle Tracking Analysis (NTA), a technology based on the same principles of DLS: light scattering and Brownian motion. The instrument used for this type of analysis is NanoSight NS300 (Malvern Panalytical) which, as all NTA systems, is specifically designed to rapidly measure the concentration and the hydrodynamic radius of nanoparticles ranging from 10 to 2000 nm, with a higher resolution than DLS systems. In fact, the NPs are loaded in a microfluidic system, and pass through a transparent chamber, where they are hit by a laser beam, which scatters and is detected by a 20x magnification microscope, connected with a video camera. The camera has a frame rate of 30 frames/s, allowing to capture Brownian motions of the NPs and to track them individually. Based on the recorded video, the instrument relative software is

able to calculate hydrodynamic radius using Stokes Einstein (equation 3) and to evaluate size distribution and concentration of the nanoparticles.

2.2 Drug loading

Drug loading protocol optimization has been one of the steps of this Master's thesis in which much effort was made. The main challenge is in fact to encapsulate a satisfying amount of AGI-6780, which is extremely hydrophobic, in the silica core of the NP. Basically, the MSNs are centrifuged at 10000 RFC for 5 minutes and the supernatant is discarded. In the meanwhile, an aliquot of 10 mM AGI-6780 (Selleckchem, Munich, Germany), which is stored at -80 °C, is thawed and diluted in dimethilsulphoxide (DMSO) and water to obtain a 1mM AGI-6780 solution.

Different concentrations of DMSO and water were tested: firstly, the drug was diluted with DMSO alone; successively, water (MilliQ bidistilled) was added to DMSO in various proportions to obtain 50:50, 60:40, 70:30, 80:20 and 90:10 in volume DMSO:H_2O solutions. The DMSO-water-AGI-6780 solution (called in the following "loading solution") are prepared adding first DMSO to the drug and then adding drop by drop water, maintaining the vial in contact with ice. In fact, when water is mixed with DMSO an exothermic reaction occurs and the temperature needs to be reduced, in order to prevent drug from denaturation or damage.

The pellet is resuspended in one of these loading solutions, maintaining a ratio of 400 µL per mg of MSNs. The particles are stirred at 350 rpm for 1h at room temperature.

UV-visible spectroscopy: AGI-6780 concentration evaluation

To evaluate the amount of drug encapsulated in the MSNs, UV-Vis (Ultraviolet–Visible) Spectroscopy was employed: the used device is Thermo Scientific Multiskan FC and with its relative software, Thermo Scientific Skanit. UV-vis spectroscopy measures the concentration C of a certain absorbing substance (a chromophore) in a solvent, according to Lambert-Beer law:

$$A = \varepsilon \cdot C \cdot l \qquad\qquad (6)$$

A is the absorbance, ε is the molar absorptivity of the analyzed chemical specie at a particular wavelength, and l is the length (in cm) of the optical path through the sample, covered by the electromagnetic radiation. The absorbance of the sample at a given wavelength is calculated as the logarithm of the ratio between incident radiation intensity (I_0) and the transmitted radiation intensity (I):

$$A = log\left(\frac{I_0}{I}\right) \qquad\qquad (7)$$

In fact, the sample is hit by an electromagnetic beam at a selected wavelength in the UV and visible range (from 100 to 800 nm). Part of the radiation is absorbed by the chromophore and part of it is transmitted and continues its path towards the detector, where it is collected.

Before starting with any evaluation of loaded drug, to assess the relationship between the concentration of AGI-6780 and the output absorbance value, calibration curves were extracted. AGI-6780 shows an absorbance peak at 283 nm, therefore all the measurements were performed at this particular wavelength. In order to obtain the calibration curves, a series of drug solutions at a known concentration were prepared, loaded in a 96 well quartz-glass plate (Hellma™, Hellma Optiks, Jena, Germany) and then analyzed through UV-vis spectrometry. The acquired values were plotted and linearly fitted with Origin software, obtaining the following equations:

Table 2.1 *Calibration curves for the different drug solutions; y is the absorbance value (dimensionless) and x the relative concentration [μM].*

AGI-6780 loading solution	Equation
100% DMSO	$y = 0.00298 \cdot x + 0.02576$
50% DMSO 50% water	$y = 0.00077 \cdot x - 0.12026$
60% DMSO 40% water	$y = 0.00305 \cdot x - 0.01229$

Loaded drug evaluation

The estimation of the amount of drug encapsulated in MSNs, expressed in terms of concentration (µM) was made through an indirect method: it is calculated as the difference between the concentration of AGI-6780 in the loading solution before and after having exposed MSNs to it and stirred for 1h. during the loading procedure, in fact, 200 µL extra of loading solution are prepared and put aside to use it later as control solution (CS). 100 µL of DMSO-water solution (blank solution, BS) in the same proportions as the loading solution are prepared to establish a background absorbance value. After the loading process, the NPs are centrifuged at 10000 RCF for 5 minutes and then the supernatant is collected. The 96 wells quartz plate is loaded with BS, CS and the supernatant and analyzed trough UV-vis spectroscopy.

The concentration of the drug loaded in MSNs (C_{MSN}) is calculated through the following formula:

$$C_{MSN} = C_{CS} - C_{sup} \tag{8}$$

Where C_{CS} and C_{sup} are the concentrations of AGI-6780 in the control solution and in the supernatant respectively and are both calculated as the concentration value corresponding to their normalized absorbance value, which is obtained through subtraction of the absorbance of the blank solution to the absolute absorbance:

$$C_{CS} = \frac{A_{CS} - A_{BS} - q}{m} \tag{9}$$

$$C_{sup} = \frac{A_{sup} - A_{BS} - q}{m} \tag{10}$$

Where q and m are the intercept and the slope of the calibration curve.

Left drug evaluation

To assess the quantity of drug remaining in the nanocarriers after stability or release tests, the pelleted MSNs were resuspended in DMSO (200 µL per mg) and

sonicated for 3 minutes. Sonication is a fundamental step in this process, because it provokes the release of the eventually remained drug from the mesoporous silica pores. NPs are successively centrifuged at 10000 RCF for 10 minutes and the supernatant is collected. The resulting pellet is resuspended again in 200 µL DMSO per mg of MSNSs and sonication and centrifugation steps are repeated. The collected supernatants are mixed and analyzed through UV-vis spectroscopy. The described steps are performed in parallel both for loaded and unloaded MSNs, used as control. In fact, the absorbance value of unloaded NPs is subtracted to the loaded NPs one, as a background which takes into account lipidic and silica fragments, that may generate a variation in the absorbance values.

2.3   Lipidic coupling

To create the protocell structure, a lipidic bilayer was formed on drug-loaded MSNs thanks to solvent exchange method. For this purpose, an optimized mixture of synthetic lipids was prepared combining 100 µL DOPC (1,2-dioleoyl-sn-glycero-3-phosphocholine from Avanti Polar Lipids Inc.) in chloroform, corresponding to 2.5 mg of lipids, 1 mg of cholesterol, and 32.8 µL DSPE-PEG-NH$_2$ (1,2-distearoyl-sn-glycero-3-phosphoethanolamine-N-aminopolyethylene glycol) in chloroform, with corresponding weight of 0.328 mg. The mixed lipids are left under the fume hood until complete evaporation of the chloroform. Once dried, the lipids are rehydrated with 1 mL ethanol-bidistilled water solution (60% H$_2$O and 40% EtOH in volume). With these concentrations, the solution allows the lipids to stay dispersed as single macromolecules, preventing their aggregation and the formation of micelles. The lipid mixture is stored at 4°C to avoid ethanol evaporation and consequent modification of the relative concentrations in the solution.

The coating of the MSNs is performed adding 100 µL of the lipid mixture to 1 mg of pelleted MSNs (which can be either precedingly loaded with drug or void to obtain control samples) and vigorously pipetted. Then, 900 µL of bidistilled water (lipid mixture-water ratio is fixed to 1:10) is quickly added and the sample is pipetted again with the same tip employed to add the lipids. The sample is then vortexed for approximately 30 s. The addition of water unbalances the proportions between ethanol and water; the lipids, exposed to this enhanced volume of water,

rearrange forming bilayers on the MSNs (lipidic shell). This is a self-assembly process, where the hydrophilic heads of the lipids tend to arrange towards the surface of the silica and the water itself, whereas the hydrophobic tales "hide" between the two layers of hydrophilic heads, the farther possible from water or hydrophilic surfaces.

To obtain a sterile lipidic mixture (used to prepare the samples destined to cell culture), the dried lipids are rehydrated in 400 µL of ethanol and successively, under biological hood 600 µL of sterile bidistilled water (autoclaved and filtered with 0.1 µm filter syringe) is added. In this case, all the MSNs coating procedure is performed under biological hood and 900 µL of sterile bidistilled water is added.

Table 2.2 *Formulation of the lipidic shell*

	DOPC	Cholesterol	DSPE-PEG-NH$_2$
Molecular Weight (g/mol)	786.1100	386.6500	2790.5210
Molar ratio (%)	55	44	2
Weight (mg)	2.5	1	0.328
Corresponding volume (µL)	100	/	32.8

2.4   Dialysis

Lipid-coated MSNs are dialyzed in Phosphate Buffer Saline (PBS) in order to remove the non-encapsulated drug from the MSNs. This process is also useful to improve the uniformity of the lipidic shells and the distribution of the nanoparticles. It consists in loading 1 mL of coated nanocarriers (which are dispersed in water-ethanol-solution of the coating process) into a dialysis membrane (SnakeSkin dialysis Tubing 3.5K MWCO, 16 mm dry I.D., 35 feet by Thermofisher Scientific). The tubing is previously cut into 10 cm approximately and soaked in PBS, in order to hydrate it, make it easier to handle and to allow the closure of one extremity by a knot. Once the sample is loaded, the other extremity is knotted and eventually tagged with a clip (if more than one sample is prepared). The tubing is then inserted

in a jar filled with PBS (a ratio of about 0.5 L per mg MSNs is maintained), which is placed onto a stirring plate and 20 hours of stirring at 70-80 rpm are executed. In the case of sterile samples, the whole procedure before the sealing of the jar is performed under biological hood and sterile PBS is employed.

2.5   Fluorescence microscopy

Fluorescence microscopy is a microscopy technique relied on the fluorescence phenomenon: particular specimens, called fluorophores, are able to absorb light in a particular wavelength band and re-emitting it nearly simultaneously. Fluorescent dyes are special fluorophores developed to specifically bind to a target (typically a molecule or a functional group) and to absorb and re-emit the radiation in characteristic wavelength ranges at well-defined intensities. Dyes with different absorption and emission bands can therefore be employed contextually, opening the possibility to work with multiple channels. In fact, fluorescent microscopes, are provided with multichannel system, which irradiates sequentially the specimen at the wavelength bands that specifically excite the fluorophores and then separate (through a filter) the light emitted by the fluorophores. Exploiting this mechanism, samples can be colored with multiple dyes, each one labelling a different element; fluorescence microscopes give hence the possibility to visualize and localize both separately and together the various fluorophores in the specimen, allowing multichannel colocalization analysis. Modern epi-fluorescent microscopes can contextually perform fluorescence and transmitted light microscopy.

For all the analysis a wide-fluorescence inverted microscope (Nikon Eclipse TiE), equipped with a super bright wide spectrum source (Shutter Lambda XL) and a high-resolution camera (Zyla 4,2 Plus, 4098x3264 pixels, Andor Technology) was employed. The images were taken with the 100x immersion oil objective (Apo 1.40, Nikon).

Colocalization analysis

To qualitatively evaluate if the nanoconstructs were correctly assembled, fluorescence microscopy was performed, labelling MSNs, lipids and eventually the

antibodies with different fluorescent dyes. Each dye has its own absorption and emission range, so that the labelled elements are visible in different channels. When the fluorescent spots of different channels coincide in space, are defined "colocalized", meaning that with great probability they not only are overlapped in the acquired microscopy image, but they also truly locally coincide. Colocalization analysis is performed on the multichannel images taken and consists in selecting through a software (in this case NIS-element software) a set of spots for each channel, according to their emitted light intensity. Then the software highlights and counts all the spots present in the same point of the picture in every channel considered. The percentage of colocalized nanoparticles is defined as the number of colocalized spots in relation to the number of spots of MSNs (i.e., only the core of the nanoparticles) channel:

$$\%colocalization = \frac{n.\,colocalized\ spots}{n.\,MSNs\ cores}\ \% \tag{11}$$

Various dyes were employed over this work; Atto 647 or Atto 550 NHS-ester (Sigma Aldrich) were used for MSNs labelling, since NSH-esters bond covalently to the amino groups present on silica surface (thanks to MSNs superficial functionalization). DiO (DiOC$_{18}$(3) (3,3'-Dioctadecyloxacarbocyanine Perchlorate)) or DiD (DiIC$_{18}$(5) solid (1,1'-Dioctadecyl-3,3,3',3'-Tetramethylindodicarbocyanine, 4-Chlorobenzenesulfonate Salt)) were employed for the lipids. These two dyes are in fact lipophilic and incorporate in the lipidic shell, after a short incubation. The used dyes and their absorbing and emitting characteristics are listed in Table 2.3.

Table 2.3 *List of employed fluorescent dyes with their respective characteristics.*

Dye	Colored element	Excitation peak (nm)	Emission peak (nm)	Channel
Atto 550 NHS-ester	MSNs	554	574	**Red**
Atto 647 NHS-ester	MSNs	643	665	**Far Red**
DiO	Lipids	484	501	**Green**
DiD	Lipids	644	665	**Far Red**

.

Antibodies were colored exploiting a secondary antibody which is linked with coumarin, (as explained in the following paragraphs).

MSNs and lipidic shell: 2-channel colocalization

For simplicity, here it is reported the 2-channels colocalization protocol, which has the aim to evaluate the quality of MSNs lipidic coverage. Also, the 3-channel analysis was performed, when antibody was included in the formulation. This process is described in the functionalization section.

In order to colour silica cores, 1 mg MSNs were dispersed in 1 mL ethanol and 2 µL Atto were added. The vial is then covered with aluminium foil (since the dye is photosensitive and fades with exposure to light) and stirred overnight at 200 rpm. The following day the MSNs are centrifuged for 5 minutes at 10000 RCF and the conventional coupling procedure and following dialysis is performed, having only a variant: every step of this procedure was carried out avoiding the exposure of the sample to light sources; for this reason, also the jar for the dialysis was covered with aluminium foil. After dialysis, and immediately before fluorescence microscopy, the extracted nanoconstructs were coloured with 0.5 µL DiO or DiD and incubated in orbital shaker at 37°C for 30 min at 200 rpm. For microscopy analysis, 5-10 µL drops of sample were laid onto a microscope slide and sealed with a cover glass and small drops of nail polish in the angles. The slide was then turned upside-down and inserted in the glass holder, after having covered the microscope objective lens with a drop of silicone oil.

2.6   Stability tests

The aim of this analysis is to understand the behaviour of the nanoconstucts at the storage conditions, i.e., NPs in PBS at room temperature and static condition. It is in fact extremely important to know if in the first hours after the preparation of the NPs, drug leakage occurs and, in case of affirmative answer, with which kinetics and which quantities of drug the loss happens. For this purpose, 0.5 mg samples of loaded and unloaded MSNs (used as control samples), after drug loading evaluation, were coupled with lipids and dialyzed, following the steps described in

the previous paragraphs. After 20 h of dialysis, the samples were extracted and centrifuged at 10000 RCF for 5 minutes. the supernatant was collected (leaving a meniscus on the pellet to prevent them from drying) and analyzed through UV-Vis spectroscopy. The samples were then resuspended in 500 µL PBS each, maintaining the concentration of 1 mg/mL. The time when the resuspension of NPs was completed, was considered as the time zero. At scheduled time steps of 1h, 4h, 24h, 48h, 72h, 96h (4d), 144 (6d) and 168h (7d) the evaluation of drug concentration was performed, as described in the following. Successively, the time steps were reduced to 1h, 4h, 24h, since it was noticed that leakage occurred mainly in the initial 24h and the delivered nanoparticles are employed in MBC laboratories within 24h. For every time step, the samples were centrifuged, the supernatant was collected and analyzed; the supernatant was then recovered from the multi-well plate and put together again with the pelleted sample and vortexed. At the end of this process, the NPs were destroyed through sonication to evaluate the quantity of drug still inside the MSNs (see relative paragraph). This was also done to verify if the cumulative drug leakage measured throughout the stability test is compatible with the drug left in the silica and the starting loaded drug amount.

To calculate the concentration of the drug in the supernatant collected at the various time points, a calibration curve was obtained ad hoc from a set of absorbance values of AGI-6780 in PBS at known concentrations. The equation resulting from linear fitting of the concentration-absorbance points is:

$$y = 0.00174 \cdot x - 0.00353 \tag{12}$$

Where y is the absorbance value and x the concentration (µM).

AGI-6780 in PBS: calibration curve

Equation	y = a + b*x
Plot	normaized absorb
Weight	No Weighting
Intercept	-0,00353 ± 0,0019
Slope	0,00174 ± 4,7095
Residual Sum of Squ	1,14142E-4
Pearson's r	0,99781
R-Square (COD)	0,99563
Adj. R-Square	0,9949

Figure 2.4 *Calibration curve employed for stability test: AGI-6780 in PBS. The absorbance values relative to 0, 1, 2.5, 5, 10, 25, 50 and 100 μM concentration points were linearly fitted using OriginPro software.*

2.7 Release tests

Another important step is to understand how the nanoparticles behave in cell culture conditions; for this reason, release tests in acellular environment, i.e., in cell culture medium (RPMI 1640, EuroClone, Pero, Italy), at 37 °C were carried out. 0.5 mg MSNs were loaded with AGI-6780, coupled with lipids and dialyzed. In parallel, coupling and dialysis was performed for 0.5 mg uncoated MSNs, which served as control samples. After dialysis, the samples were centrifuged at 10000 RCF for 5 minutes and resuspended in 500 μL RPMI each. 100 μL aliquots were collected from these samples to obtain 5 vials of loaded NPs and 3 vials of unloaded control NPs. 900 μL RPMI was added in every vial to achieve a 100 μg/mL MSNs final concentration. The samples were placed in orbital shaker at 37 °C and 200 rpm speed, together with 3 vials filled with 1 mL RPMI each, used as color comparison in case of suspected bacterial contamination of the samples (RPMI changes color, turning from bright pink to opaque yellowish when contaminated by bacteria).

Similarly to stability test, at selected time points: 2h, 4h, 6h, 24h, 48h, 72h, 96h (4d), 144 (6d) and 168h (7d) the samples were centrifuged (10000 RCF, 5 min), the supernatant was all collected (leaving only a meniscus) to stop drug release and put in temporary vials, from which four 100 µL aliquots for each sample were extracted and loaded in the quartz multi-well for UV-vis analysis. The supernatant was then recollected from the plate and put together with the remaining RMPI in the temporary vial and inserted again in the respective original NPs vial. As in the case of stability test, a specific AGI-6780 in RPMI calibration curve was calculated:

$$y = 0.00689 \cdot x - 0.00988 \tag{13}$$

Where y is the absorbance value and x the concentration (µM). Also in this case, after the last time step, the NPs were destroyed in order to estimate the amount of drug still encapsulated after a week of release.

AGI-6780 in RPMI: calibration curve

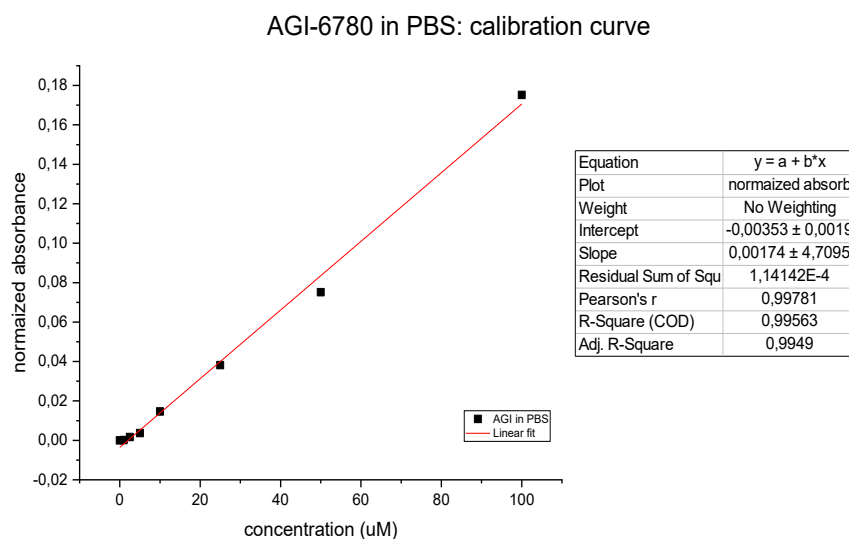| Equation	y = a + b*x
Plot	normalized absorba
Weight	No Weighting
Intercept	0,00988 ± 0,00901
Slope	0,00689 ± 3,92654E
Residual Sum of Squa	0,00123
Pearson's r	0,99357
R-Square (COD)	0,98719
Adj. R-Square	0,98399
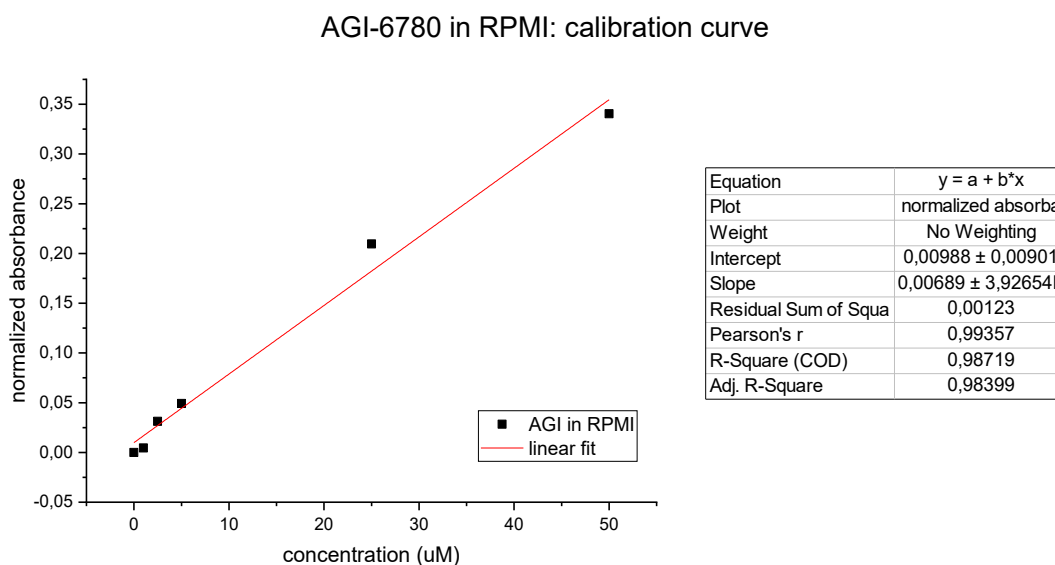
Figure 2.5 *Calibration curve employed for release test: AGI-6780 in RPMI. The absorbance values relative to 0, 1, 2.5, 5, 25 and 50 µM concentration points were linearly fitted using OriginPro software.*

2.8 Hemocompatibility tests

Hemocompatibility test consist in the evaluation of the time necessary for plasma to coagulate, in presence of nanoparticles. Normally, plasma is treated with anticoagulants (in this case plasma citrate), in order to prevent coagulation and allow its proper storage and employment. Here, the anticoagulant effect of plasma citrate was overridden by calcium chloride ($CaCl_2$, 25 mM). In this experimentation, 2 identical sets of samples were analyzed contextually: one was treated with calcium chloride and showed coagulation, the other was left without calcium chloride and used as control. 2 types of nanoparticles samples were prepared: the first consisted of MSN alone, in the other MSNs were coated with lipidic bilayer and dialyzed for one night, as usual. Both samples were washed 2 times with water and then centrifuged (10000 RCF for 5 min). Under biological hood, each pellet was resuspended in 1 mL of a 0.1 µm filtered physiological solution. Samples were then diluted with physiological solution to obtain 2 concentrations each: 100 µg/mL and 50 µg/mL. After sample preparation, a vial of 5 mL plasma, that was stored at -20°C, was thawed in a 37°C bath. 3 mL calcium chloride were heated in 37°C bath as well.

Under hood, samples were loaded in a treated 96 well plate as described as follows. 12 types of well were prepared (6 treated with $CaCl_2$, and 6 not), each of them was repeated in triplicate, obtaining a total of 36 wells (see Table 2.4). Every well was loaded with 75 µL plasma and then, where scheduled, 75 µL of physiological solution or sample was added and the completed plate is put in incubator at 37°C for 5 min. Following, 150 µL calcium chloride were quickly added with a multichannel pipette and immediately after the plate was inserted in UV-vis spectrometer (formerly heated at 37°C) for analysis.

The analysis protocol followed (plasma clotting protocol) consists in the periodical reading of the plate: a measure is taken every 30 s for 45 minutes. During this time, the plate is incubated at 37°C. The analyzed wavelength is 405 nm.

Table 2.4 *Scheme for plate loading*

Samples (x3 wells)		Plasma (µL)	Physiological solution (µL)	MSNs Samples (µL)	Calcium chloride (µL)
CONTROLS	Plasma	75	/	/	/
	Plasma + physiological solution	75	75	/	/
	Uncoated MSNs 50 µg/mL	75	/	75	/
	Uncoated MSNs 100 µg/mL	75	/	75	/
	LB-coated MSNs 50 µg/mL	75	/	75	/
	LB-coated MSNs 100 µg/mL	75	/	75	/
CaCl₂-treated samples	Plasma	75	/	/	150
	Plasma + physiological solution	75	75	/	150
	Uncoated MSNs 50 µg/mL	75	/	75	150
	Uncoated MSNs 100 µg/mL	75	/	75	150
	LB-coated MSNs 50 µg/mL	75	/	75	150
	LB-coated MSNs 100 µg/mL	75	/	75	150

2.9   In vitro tests

In vitro tests were carried out by research group of Prof. Roberto Piva in MBC laboratories (Molecular Biotechnology Centre, University of Torino), as proof of concept for the efficacy of the drug delivery capabilities of the nanosystems developed and for the synergistic action of AGI-6780 (loaded in the MSNs) with free CFZ. The dyalized lipid-coated MSNs, dispersed in the dialysis solution at an estimated concentration of 1 mg/mL, were delivered to MBC immediately after extraction from dialysis and employed for cell viability test on KMS-28 human multiple myeloma cell line (LGC stand, American Type Culture Collection authenticated).

More in details, KMS-28 cells are maintained in RPMI 1640 medium (EuroClone, Pero, Italy), supplemented with 2 mM of L-glutamine, 100 U/mL of penicillin, 100 μ g/mL of streptomycin (Gibco), 10% fetal bovine serum (FBS; SigmaAldrich, St. Louis, Missouri, USA), and grown at 37°C in humidified atmosphere with 5% CO_2

Cell viability test

To assess the cytotoxicity of the NPs in combination with CFZ, KMS-28 cells are treated with NPs, loaded with AGI-6780 and void (used as control samples) and CFZ. Different concentrations of NPs and CFZ were tested. Cells were seeded in a 24-well plastic plate with a concentration of 100,000 cells/mL and volume was brought to 1mL with RPMI 1640 culture medium. NPs were centrifuged at 10000 RCF for 5 minutes and pellets were resuspended in 100 µL of RPMI. After 10 minutes, the solution was diluted to obtain 10 mg/mL, 5 mg/mL and 2.5 mg/mL NPs concentrations.

Several protocols were tested, and experiment were conducted varying NPs and drug concentrations as well as the time steps for drug treatment and FACS analysis. A scheme of the characteristics of the various protocols is reported in the table below. To assess the validity of the biological tests, experiments should be done at last in triplicate (n=3). Of the test performed NP12, NP13 and NP14-double form a triplicate experiment since the treatment conditions are the same. In the following, a methodology common to all experiments is described.

Table 2.5 *Scheme of cell viability test protocols*

Test	-24h	Time 0	+2h	+6h	+48h	+72h	+5d	+7d
NP8		Cells seeding + NP	CFZ		FACS			
NP9		Cells seeding + NP	CFZ				FACS	
NP11		Cells seeding + NP	I CFZ			II CFZ	FACS	
NP12	Cells seeding + NP	II NP	CFZ					FACS
NP13	Cells seeding + I NP	II NP	CFZ					FACS
NP14 single	Cells seeding + NP/free AGI		CFZ		FACS		FACS	
NP14 double	Cells seeding + I NP/free AGI	II NP	CFZ		FACS		FACS	
NP15		Cells seeding + NP/free AGI		CFZ	FACS	FACS	FACS	
NP16		Cells seeding + NP/free AGI		CFZ	FACS	FACS	FACS	FACS

The experiments started with the treatment of seeded cells with NPs solutions: 10 µL of NPs (both loaded and unloaded) at different concentrations or free AGI-6780 (5 µM, starting from NP14 experiment) were added. Starting with NP12 experiment, the cells were treated again with NPs 24h after the first dose. The time the second (in case of 2 NPs doses) or the first (in case of a unique dose of NPs) was performed, was called "time zero". 2 hours (NP8-14) or 6 hours (NP15-16) after time zero, cells were treated with free CFZ solutions (5 mM, 5 µM, 500 nM, 250 nM and 125 nM in DMSO). A second free CFZ treatment was performed after 72h in NP11 experiment. At various time points (48h, 72h, 5d or 7d), cell viability was analyzed through Fluorescence-activated cell sorting (FACS) flow cytometry method; the instrument used was BD FACS Celesta cytofluorimeter (BD Biosciences). For flow cytometry assay, 300 µL of cells were collected and 1 mL of PBS was added. Cells were centrifugated at 1300 RCF for 4 minutes, at RT and the

supernatant was discarded. Cells were resuspended in 100 µL Annexin V Binding Buffer and trated with TMRM (tetramethyl rhodamine methyl ester from Molecular Probes, diluted 1:1000). After every FACS measurement, 1 mL of RPMI was added to each well.

2.10 Functionalization

Antibody reduction

Antibody reduction is performed for the purpose of breaking the disulfide bonds and exposing thiol groups (-SH), which can be bound to a maleimide-functionalized lipid, DSPE-PEG$_{2000}$-maleimide (Avanti Polar Lipids Inc.), through the reaction represented in Figure 2.6.
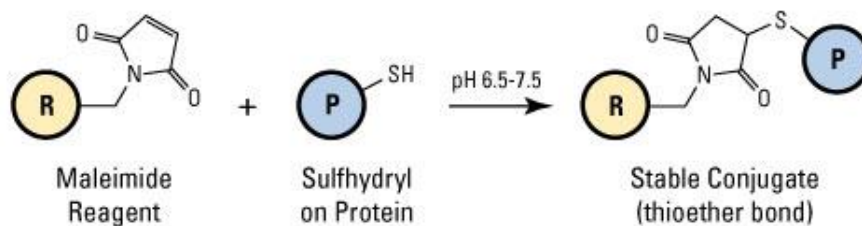
Figure 2.6 *Covalent bonding between thiol group exposed by antibody fragments and maleimide group present in DSPE-PEG2000-maleimide lipids.*

The chosen reducing agent is TCEP (Tris[2-carboxyethyl] phosphine hydrochloride II, Disulfide Reducing Gel, by Thermofisher), employed in combination with EDTA (Ethylenediaminetetraacetic acid), which prevents the reduction-resulting fragments to recombine. The reduced antibody is the Anti-CD38 Daratumumab (20 mg/mL), which is a human immunoglobulin FDA-approved for clinical purposes. Daratumumab was aliquoted diluting 5 µL of stock solution 1:20 in a 10 mM EDTA solution in PBS, obtaining 100 µL of Daratumumab solution concentrated 1 mg/mL, which were then reduced with TCEP, proceeding as follows.

200 µL TCEP were centrifuged in a 1.5 mL spin cup at 1000 RCF for 30 s, the flow through was then discarded and the filter with TCEP was placed in a new spin cup container. Daratumumab was subsequently added by delicately pipetting the solution in the gel and gently vortexing. The spin cup was sealed with parafilm

to avoid any leakage and then placed in a rotating wheel; the sample was left in rotation for 24h. At the end of the 24 hours, the sample was centrifuged at 1000 RCF for 1 min; the flow through was in this case collected, as it contains the reduced antibody.

Gel electrophoresis

In order to verify if Daratumumab has actually been reduced, a Sodium Dodecyl Sulphate – Polyacrylamide Gel Electrophoresis (SDS-PAGE) was performed. This technique relies on the use of polyacrylamide gels, which can have different pore sizes, depending on the level of crosslinking of the acrylamide monomers. The principle is that proteins, in this case represented by antibodies and antibody fragments, move from one side of the gel to the other (a potential difference is applied) and stopping in a particular point, according to their molecular weight. In fact, SDS form complexes with proteins, which get linearized and their native charges are shielded with the negative charges of SDS molecules. In this way, a rod-like shape and a similar mass-to-charge ratio is conferred to proteins, which are thus able to travel inside the gel and be separated according to their molecular weight, when a voltage is applied.

To perform gel electrophoresis, a precast gel was used (Criterion TGX stain free precast gel 12+2, 45 µL wells, 4-15% by Bio-Rad) and 3 wells were loaded: the first with a whole antibody sample (A), the second with a marker (precision plus protein dual color standard by Bio-Rad), which is a mixture of proteins with known molecular weight that serves as reference (M) and the third with the reduced daratumumab (B).

Sample preparation

Sample A was prepared adding 2.25 µL of Daratumumab (1 mg/mL) in 24.75 µL PBS; for sample B, simply 27 µL of the solution collected after reduction with TCEP were used. 9 µL sample buffer (4x Laemmli Sample Buffer) were added to each sample. An extra vial was prepared with a solution of water and sample buffer maintaining a volume ratio equal to 3:1. This water sample (X) is used to separate sample lanes. To complete the preparation of the samples, are heated in a thermoblock, at 95°C for 10 minutes.

Table 2.6 *Gel loading scheme*

Well	1	2	3	4	5	6
Gel Layout	A	X	M	X	B	X
Sample (µl)	27	/	/	/	27	/
Marker (µl)	/	/	15	/	/	/
Laemmli (µl)	9	9	/	9	9	9
Water (µl)	/	27	/	27	/	27

Cell assembly and electrophoresis run

Running buffer was prepared mixing 70 mL of 10x Tris/Glycine SDS and 630 mL bidistilled water. The precast gel was extracted from its package and inserted in the designated slot of the electrophoresis cell (Criterion Cell); the upper and the lower chamber of the cell were filled with the running buffer. The samples were loaded in the gel (A total of 6 wells were loaded with 36 µL each), following the layout reported in table. Then, the cell was closed and connected to the power supply (PowerPac™ Basic Power Supply), a constant 200 V voltage was set, and the electrophoresis was started. The electrophoresis ends when the blue line of sample buffer reaches the bottom of the gel and vanishes; at this moment, the power supply is turned off and the gel can be extracted.

Gel treatments

The gel was delicately extracted from its case and laid down in a container and washed 3 times with bidistilled water (5 minutes washing cycles on orbital shaker at 50 rpm). Successively, water was removed, and the gel was stained by pouring approximately 50 mL Coomassie solution (Coomassie, Bio-Safe) on it. The gel was left in shaking at 50 rpm for 1h and then washed again with bidistilled water, after having removed the stain (two washing cycles of 30 minutes each). The gel is then left in shaking overnight (the container is covered with aluminum foil). The day after, the gel is laid down on a white panel and pictures are taken.

Table 2.7 *List of the materials for gel electrophoresis*

Material	Name
Precast Gel	4-15% Criterion TGX Gel 12+2 well 45 µl
Running Buffer	**10x Tris/Glycine SDS, 1L**
Sample Buffer	**4x Laemmli Sample Buffer**
Protein stain	Coomassie, Bio-Safe,1l
Marker	Precision Plus Protein Dual Color Standard
Power Supply	PowerPac™ Basic Power Supply
Electrophoresis cell	Criterion Cell

Antibody binding

Two functionalization tests were performed, in the first of which two distinct antibody binding protocols were carried out. Both protocols have a fundamental step: the conjugation of antibody fragments with DSPE-PEG$_{2000}$Maleimide synthetic lipid. The functionalization process relies in fact on the reaction between the maleimide group and the sulphydryl groups exposed by the Ab after reduction with TCEP. The second test was performed to confirm the results of the first that were not satisfying, due to the low amounts and concentration of antibodies involved.
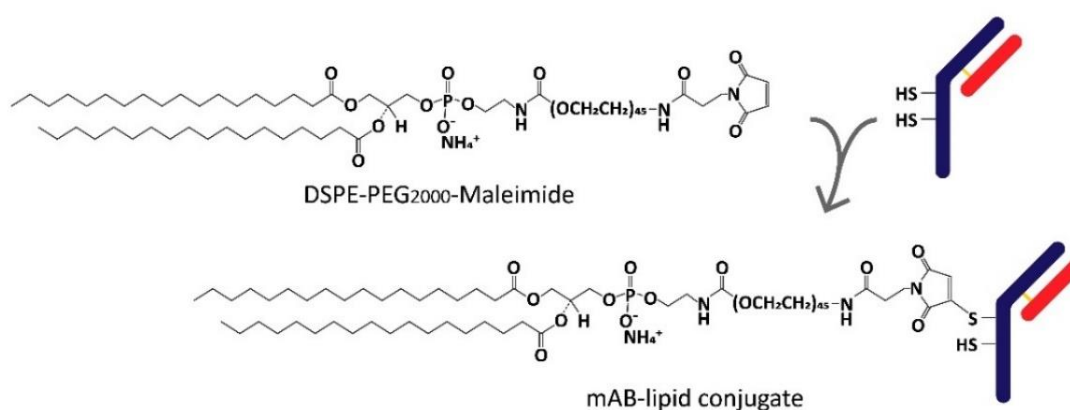

Figure 2.7 *monoclonal antibody fragment conjugates with DSPE-PEG-Mal through a thioether bond.*

Conjugation protocol

The conjugation between antibody and DSPE-PEG$_{2000}$Maleimide is performed fixing two fundamental ratios: DSPE-PEG-Mal/antibody molar ratio is fixed to 3:1 and 1:1 volume ratio is maintained between Dimethylformamide (DMF, the solvent in which DSPE-PEG-mal is dispersed with concentration 0.374 mM) and PBS (where the antibody fragments are dispersed). Depending on the estimated quantity of reduced antibody (rAb) and the present volumes, the conjugation was carried on. In the following tables, the quantities involved in the two experiments and the calculations done are summarized.

The conjugation process simply consists in combining the right quantities of reduced antibody, DSPE-PEG-Mal and antibody fragments. The obtained mixture is then shaken at 250 rpm for 1h at room temperature. After conjugation, the lipid-antibody compound can be used or stored at -20°C.

Table 2.8 *Calculations for the first antibody conjugation test.*

FIRST TEST		Relationship used
rAb volume (µL) in PBS	$20\,\mu L$	
rAb estimated amount (µg)	$3.64\,\mu g$	
rAb amount (mol)	$3.64\,\mu g/145\,kDa =$ $= 2.51 \cdot 10^{-11} \text{mol}$	
DSPE-PEG-mal amount (mol)	$2.51 \cdot 10^{-11} \text{mol} \cdot 3 =$ $= 7.53 \cdot 10^{-11} \text{mol}$	DSPE-PEG-Mal/Ab **3:1 molar ratio**
DSPE-PEG-mal volume (µL)	$7.53 \cdot 10^{-11} \text{mol}/0.374\,\text{mM} =$ $= 0.201\,\mu L$	
DMF volume to add (µL)	$20\,\mu L - 0.201\,\mu L =$ $= 19.799\,\mu L$	DMF/PBS **1:1 volume ratio**

As previously anticipated, since the amount of antibody and its concentration were too low in the first test, a second test was performed, using increasing both the amount ant the concentration of Daratumumab, for clearer results.

Table 2.9 *Calculations for the second antibody conjugation test.*

SECOND TEST		Relationship used
rAb volume (µL) in PBS	**60 μL**	
rAb estimated amount (µg)	**30μg**	
rAb amount (mol)	$30\,\mu g/145\,kDa =$ $= \mathbf{2.069 \cdot 10^{-10}}$**mol**	
DSPE-PEG-mal amount (mol)	$2.069 \cdot 10^{-10}$mol $\cdot 3 =$ $= \mathbf{6.207 \cdot 10^{-10}}$**mol**	DSPE-PEG-Mal/Ab **3:1 molar ratio**
DSPE-PEG-mal volume (µL)	$6.207 \cdot 10^{-10}$mol$/0.374\,$mM $=$ $= \mathbf{1.659\,\mu L}$	
DMF volume to add (µL)	$60\,\mu L - 1.659\,\mu L =$ $= \mathbf{58,34\,\mu L}$	DMF/PBS **1:1 volume ratio**

The subsequent step is the insertion of the DSPE-PEG-Mal-Antibody complex in lipidic shell of the nanoparticles. This can be achieved in different ways, with respective advantages and drawbacks, discussed below. The MSNs used in the following procedures were labelled with Atto 550 or Atto 647, to allow a successive check of the correct assembly of the nanoconstruct through fluorescence microscopy. For both protocols, a fixed proportion of functionalized lipidic complex was used: a quantity equals to 1% molar of the usual lipid mixture was added to the lipidic shell. For reference, in Table 2.10 are listed the amounts of lipids necessary to cover 1 mg MSNs.

Table 2.10 *Amount of lipids needed to coat 1 mg of MSNs. The sum of the quantities relative to DOPC, Chol and DSPE-PEG-amine correspond to a volume of 100 µL of lipid mixture prepared for usual MSNs coating protocol.*

	Molecular Weight (g/mol)	Weight (mg)	Amount (mol)	Molar ratio (%)
DOPC	786.11	0.25	3.18×10^{-7}	53.5
Cholesterol	386.65	0.1	2.58×10^{-7}	43.5
DSPE-PEG-NH$_2$	2790.52	0.033	1.18×10^{-8}	2
DSPE-PEG-mal	2941.642	0.0018	5.88×10^{-9}	1

Protocol 1

DSPE-PEG-mal/Antibody complex is fused with the lipidic shell (already formed around the MSNs) through incubation. For this reason, fluorescent-dyed MSNs were coupled with the usual DOPC-Chol-DESPE-PEG-amine mixture, bidistilled water was added to let the formation of the self-assembled lipidic double layer by solvent exchange (water volume was imposed to be more than 70% in volume than the sum of ethanol and DMF volumes). Only later the DSPE-PEG-Mal/Daratu-mumab complex was added, and the sample incubated in orbital shaker at 250 rpm for 4h at 37°C. After incubation, the samples were dialyzed overnight in PBS in dark conditions to avoid dye photobleaching. Quantities of antibody, MSNs and lipids used in the two experiments are listed in the tables below. MSNs amount was calculated starting from the number of desired samples and the available quantity of DSPE-PEG-Mal/Daratumumab complex.
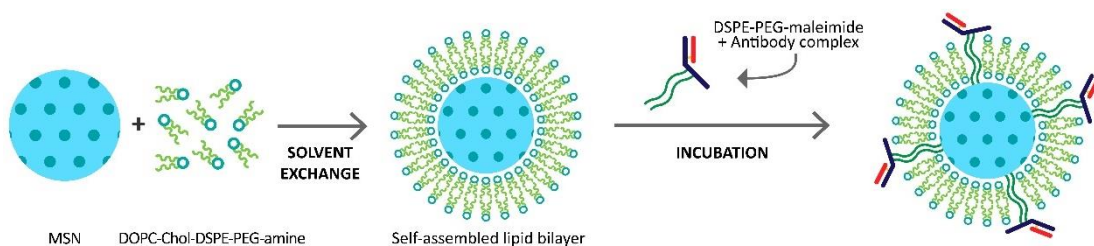
Figure 2.8 *Scheme of the first DSPE-PEG-Mal/Daratumumab complex conjugation strategy.*

This method, since the antibody/lipid complex is integrated in an already formed lipidic shell, guarantees that the antibody will be correctly exposed on the surface of the nanocarrier with high probability. On the other hand, incubation, in addition to being time consuming, can cause a considerable loss of drug.

Protocol 2

Protocol 2 is an alternative method in which incubation is avoided, allowing to immediately functionalize the nanocarriers. Basically, lipid/antibody complex is mixed with the other lipids and the shell is formed by self-assembly with the usual

solvent-exchange procedure. DOPC-Chol-DESPE-PEG-amine mixture together with DSPE-PEG-Mal/Daratumumab complex were in fact added to the labelled MSNs. Only later, the bidistilled water was added (water volume was imposed to be more than 70% in volume than the sum of ethanol and DMF volumes, as in protocol 1) to form the lipidic bilayers, this time already including the functionalized lipids. The functionalized nanocarriers are then dialyzed in PBS overnight, in dark conditions.
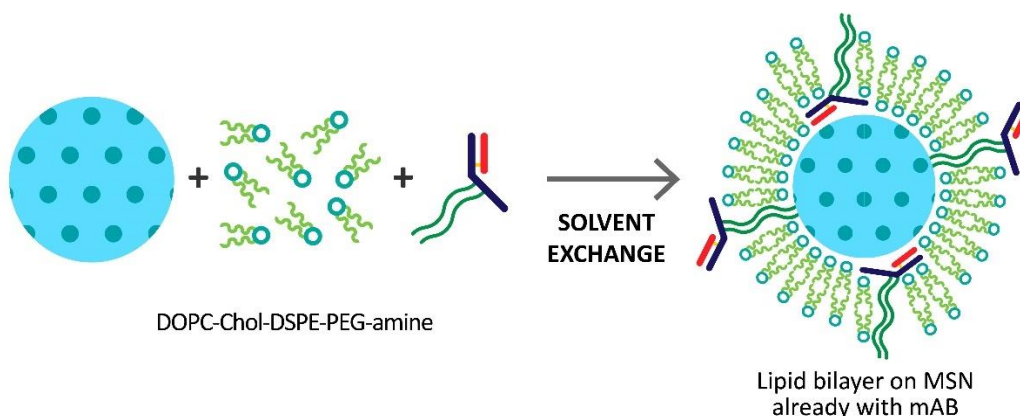
Figure 2.9 *Scheme of the second DSPE-PEG-Mal/Daratumumab complex conjugation strategy.*

Protocol 2 is faster, but it does not guarantee the correct orientation of the antibody. The right exposure of the ligand is essential for functionalization efficacy; for that reason, many antibodies (which are the most expensive component) are ineffective and thus wasted in case of incorrect orientation.

For the first test, a total of four samples of 3.2 µg MSNs each were prepared: 2 were processed following the first protocol, the other 2 following the second protocol. Each pair of samples consisted in one sample labelled with Atto550 and the other labelled with Atto647. For the second test, as a superior amount of MSNs and antibody was requested, a single sample of 50 µg Atto550-labelled MSNs was processed following protocol 1.

Table 2.11 *MSNs and lipids amount calculated for the first test.*

	volume (µL)	Corresponding amount	
MSNs	3.2	3.2 µg	
DOPC-Chol-DESPE-PEG-amine	0.32	DOPC	10×10^{-10} mol
		Chol	8.2×10^{-10} mol
		DSPE-PEG-amine	3.77×10^{-11} mol
DSPE-PEG-Mal/Daratumumab	10	DSPE-PEG-Mal	1.88×10^{-11} mol
		Daratumumab	0.63×10^{-11} mol

Table 2.12 *MSNs and lipids amount calculated for the second test.*

	volume (µL)	Corresponding amount	
MSNs	50	50 µg	
DOPC-Chol-DESPE-PEG-amine	5	DOPC	$1{,}59 \times 10^{-8}$ mol
		Chol	$1{,}29 \times 10^{-8}$ mol
		DSPE-PEG-amine	5.9×10^{-10} mol
DSPE-PEG-Mal/Daratumumab	60	DSPE-PEG-Mal	3.1035×10^{-10} mol
		Daratumumab	1.0345×10^{-10} mol

Fluorescence analysis

In order to have a visible feedback for the functionalization process, fluorescence microscopy was used to analyze the samples. Every element of the nanoconstruct was labelled with a different dye, each one showing distinct excitation and emission bands. In this way, up to three channels together were employed:

- MSNs were labelled with Atto550 (Red channel) of Atto647 (far red channel)
- Lipids were colored with DiD (far red channel) while coating Atto550-labelled MSNs or with DiO (green channel) while coating Atto-647-labelled MSNs, to avoid superimposition of signals.
- The antibody fragments were labelled exploiting a secondary antibody, which is bind to the coumarin fluorescent dye. Coumarin excitation peak is at 387 nm, and its emission peak is located at 470 nm; the dye is thus visible in the blue channel. Secondary antibody strategy was chosen to guarantee a specific interaction with Daratumumab, since the secondary antibody attaches only to the antibody binding site, also giving a proof of the correct orientation of the targeting antibody.

The samples were extracted from dialysis and put in vials covered with aluminum foil to avoid light exposure. A volume of coumarin/secondary antibody complex was added observing a 1:1 molar ratio with the Daratumumab present in the samples (no loss of antibody was considered). The samples were placed in a rotating wheel and left in rotation for 1h at room temperature. After this time, lipids were colored adding DiO or DiD, according to the dye used for the MSNs and incubated for 30 min at 37°C at 200 rpm. 5 µL drops of samples were laid onto microscopy slides and fluorescence check was performed. The images were then analyzed with the colocalization tool of the NIS-Element software.

3 Results and discussion

3.1 Mesoporous silica characterization

FE-SEM - *Field Emission Scanning Electron Microscopy*

FE-SEM analysis provided an indication on MSNs shape and size. From Figure 3.1, MSNs are indeed characterized by an overall sperical shape and diameters around 40 nm, that is consistent with analisys present in previous works [36], [41].
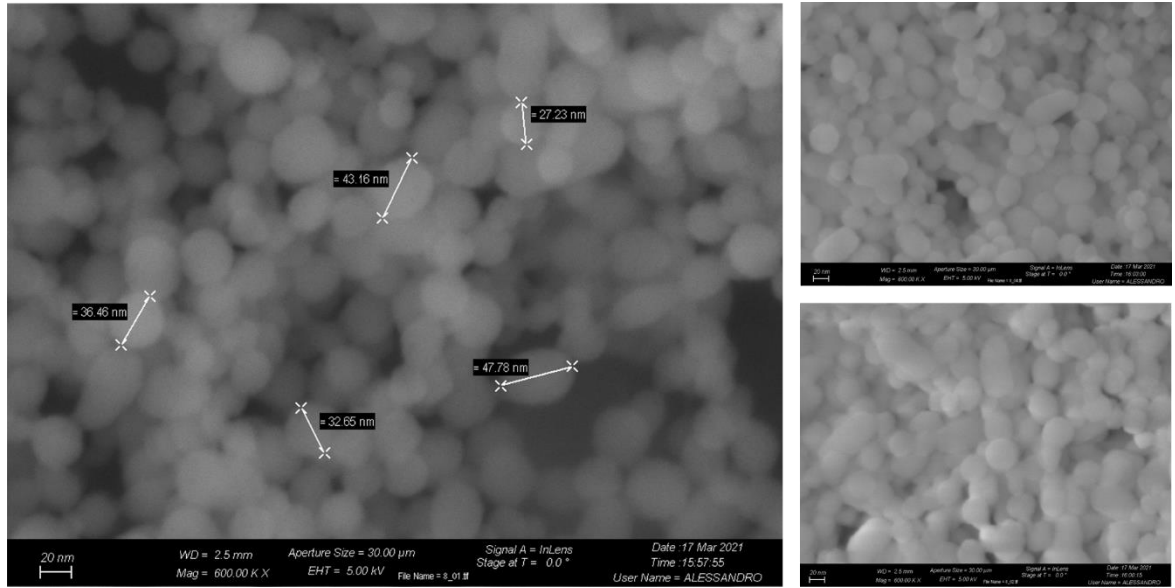

Figure 3.1 *FE-SEM images of MSNs; magnification: 600,00 K X*

Nitrogen absorption (BET)

The porous characteristics of the synthesized MSN were evaluated with BET and DFT models, starting from nitrogen adsorption and desorption isotherms, as reported in the Figure 3.2 and Table 3.1 **MSNs properties estimated through nitrogen adsorption isotherms analysis.**. The obtained isotherm shows distinctive features of type IV isotherm, typical of mesoporous materials. A first inflection point below 0.1 p/p_0 is due to microporosities in the material, then a second inflection point is present at partial pressure p/p_0 of 0.3, implicating that during the measurement, in the MSNs mesopores condensation of nitrogen has taken place.

Thirdly, an hysteresis loop is visible at higher p/p0 of 0.8, due to interparticle porosities, also called "textural porosity".

In general, above a critical pore radius and specific partial pressure of nitrogen, capillary condensation occurs: below saturation pressure, the molecules of nitrogen adsorbed at the silica surface condense in the pores in liquid form. A higher relative pressure in the adsorption branch than in the desorption phase is therefore needed.

Table 3.1 *MSNs properties estimated through nitrogen adsorption isotherms analysis.*

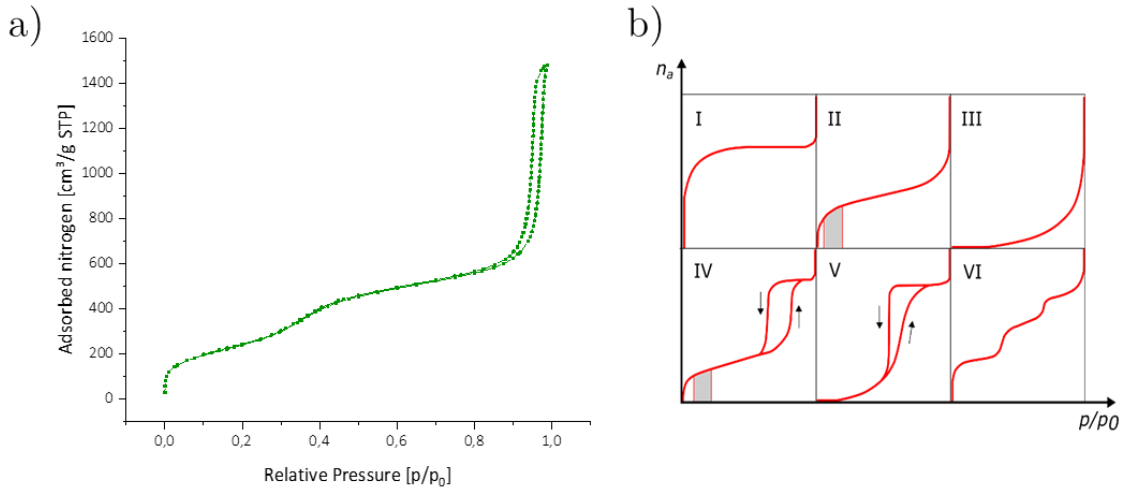|	
BET surface area	938.797 m^2/g
DFT cumulative pore volume	0.744 cm^3/g
DFT pore width	3.65 nm

Figure 3.2 *Measured nitrogen absorption isotherm plot (a). IUPAC classification of adsorption isotherms (b). n$_a$ is the adsorbed gas quantity, p/p$_0$ is the relative pressure [40]. The isotherm resulting from analysis corresponds to type IV adsorption isotherm, characteristic of mesoporous materials.*

The shape of the isotherm can be attributed to the cylindrical nature of the MSNs pores. The applied models also show the typical features of mesoporous silica

nanoparticles: specific surface of around 1000 m²/g, pore volume of approximately 1 cm³/g. The estimated diameter of pores is in the range of 3-4 nm.

Fourier-Transform infrared spectroscopy FTIR

The FTIR analysis of the sample was performed in absorbance mode, so the focus is on the vibration peak maxima present in the spectrum, as visible in Figure 3.3. The most prominent peak is the one around 1080 cm^{-1}, characteristic of the silicon oxide that confirms the silica-based nature of the nanoparticles. At 3061 cm^{-1} it is visible a small peak, which represents the isolated silanol groups, characteristic of the MSNs as well. The range between 3600 and 3000 cm^{-1} is related to stretching vibration of -OH groups, and the one between 3000 and 2800 is referred to alkyl groups (-CH$_x$) that can derive from residues of ethanol or from molecules left from the synthesis process such as surfactant molecules or from the propyl chain of the APTES functionalizing moiety. Finally, the peak at around 1600 cm^{-1} is attributed to the water bending. Water molecules from air humidity are in fact easily adsorbed onto the MSNs.
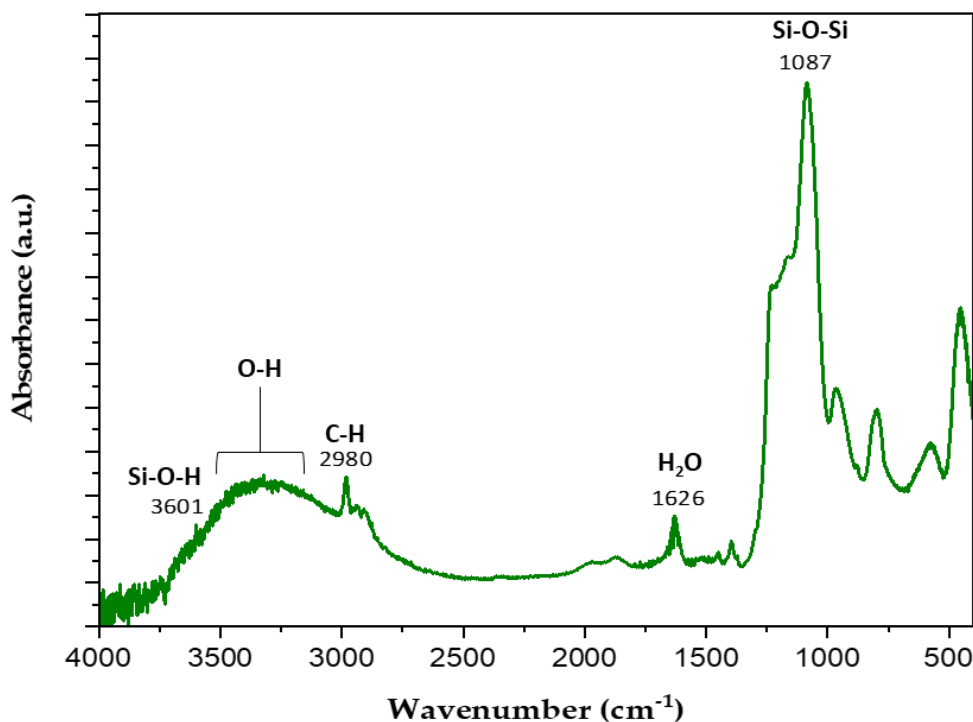
Figure 3.3 *FTIR absorbance spectrum*

Dynamic Light Scattering DLS and Zeta potential

DLS provides a measure of the hydrodynamic radius of the NPs in suspension, together with their polydispersity index (PDI), that is calculated by the software through a cumulative analysis. PDI is dimensionless and ranges from 0 (monodispersed nanoparticles, the ideal condition) and 1. PDI < 0.5 is considered a good result. The reported results in Figure 3.4 showed that the hydrodynamic radius of uncoated MSNs is different when evaluated in ethanol rather than in bidistilled water, being smaller in the first case (MSNs in EtOH: peak at 78.8 nm) and considerably bigger in the second case (MSNs in water: peak at 190 nm). This is because MSN in water have a great tendency to aggregate. Moreover, the MSNs in this work were dispersed and homogenized in the solution only by vortexing, avoiding sonication (used in previous work to disaggregate the nanoparticles), which can potentially damage the walls of pores in the mesoporous silica architecture, leading to MSNs collapse and thus to unreliable DLS data. Due to this, the curve relative to MSNs dispersed in water presents multiple peaks and a large support, and the PDI values are very high in both conditions (0.927 in EtOH and 0.985 in water), indicating a high polydispersity of NP sizes.

For what concerns MSNs covered with the lipidic shell (DOPC-Chol-DSPE-PEG coated MSNs), the hydrodynamic radius resulting from the analysis (164 nm) is lower than the one of MSNs in water (190 nm), proving that the lipidic coverage has positive effects towards colloidal dispersion and steric stabilization of the NPs, preventing MSNs from aggregation. The PDI measured in this case is in fact smaller (though still greater than 0.5) than the one of uncoated MSNs, suggesting a better distribution of the NPs sizes.

Zeta potential measurements (Figure 3.5) are helpful to understand the stability of the nanoparticles and their tendency to aggregate. In fact, the higher the superficial charge absolute value is, more the NPs will electrostatically repulse. A colloidal suspension with absolute value of zeta potential higher than 30 mV can be generally considered stable [42]. Zeta potential of the uncoated MSNs was evaluated and showed a positive charge value of 30±0.386 mV, that is between the ranges of

moderate and good stability. Positive charge is due to the protonated amino groups (-NH$_3^+$) present on the MSNs surface thanks to functionalization with APTES.

Lipid-coated MSNs shown a zeta potential of 29.0±1.3 mV, very similar to the one obtained for uncoated MSNs. Lipid bilayer is essential for the biostability of the nanoparticles, improving biocompatibility and pharmacokinetics. The LB, in fact, confers steric repulsion, preventing the MSNs to aggregate; in addition, thanks to electrically charged lipids (in this case DSPE) electrostatic repulsion is provided. A zeta potential around 30 mV, as obtained for these measurements, guarantees the good colloidal stability of the coated MSNs.
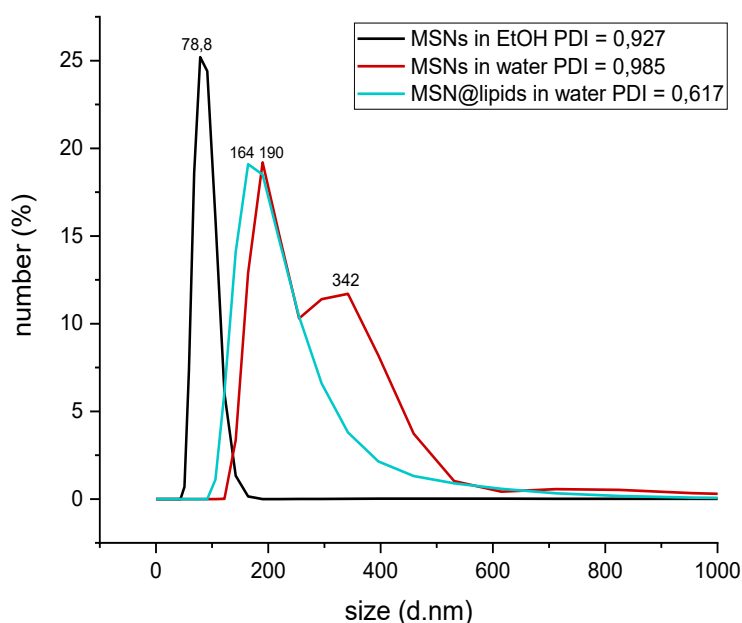

Figure 3.4 *Comparison of DLS results of uncoated MSN dispersed in ethanol or in bidistilled water and DOPC-Chol-DSPE-PEG coated MSNs in water.*
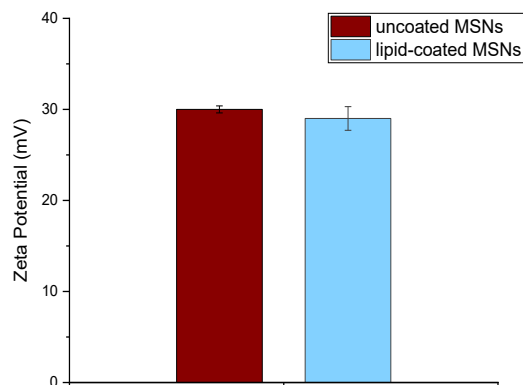
Figure 3.5 *Zeta potential results for uncoated (left) and coated (right) MSNs.*

Nanoparticle Tracking Analysis (NTA)

NTA analysis was performed on lipid-coated NPs, after being dialyzed, to have an insight of the size distribution of the nanoconstructs, in the form they are delivered to MBC for cell viability tests. NTA allows better resolution and higher accuracy than DLS, since the system has the ability to track NPs individually.
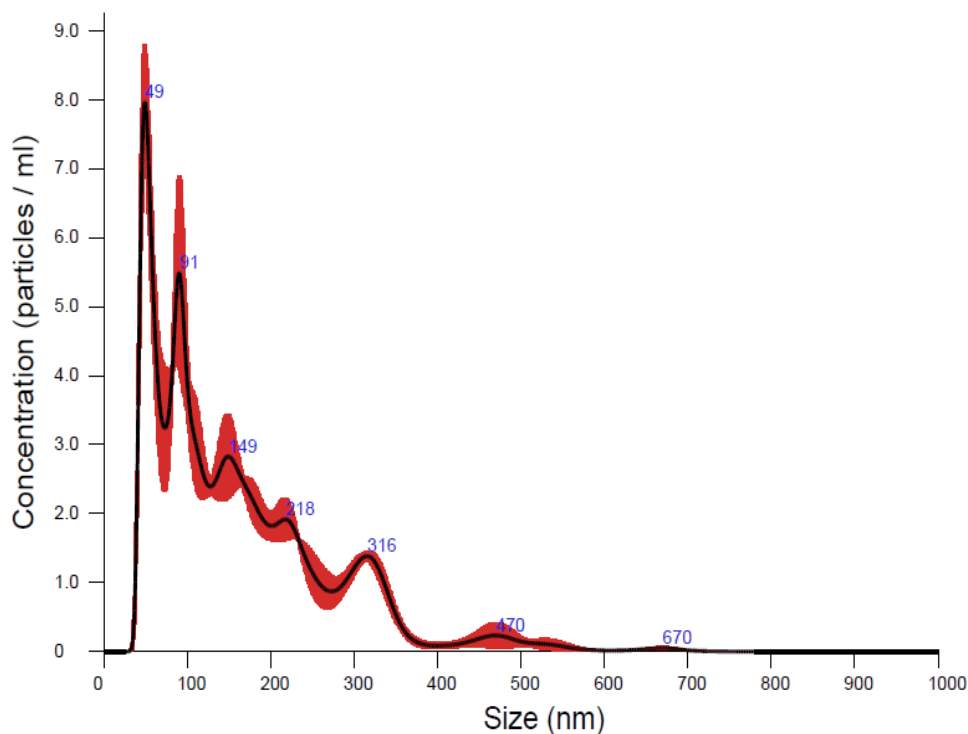

Figure 3.6 *NTA analysis of dialyzed MSNs@lipids.*

The results in Figure 3.6 show that the hydrodynamic sizes of the nanoparticles are not well distributed, having multiple peaks and a wide support of the distribution curve. The highest peak, at 49 nm, can be attributed to uncoated NP, or more likely to small liposomes that formed without encapsulating MSNs. the larger diameters can belong to agglomerates of NPs or bigger liposomes. The mean value of the sizes resulted 159.6±2.9 nm (see Table 3.2 *NTA results*Table 3.2), which is consistent with the value obtained in DLS analysis (164 nm). NTA analysis highlighted one of the main, still unresolved issues of this project, that is the poor uniformity of NPs sizes and in particular the presence of big agglomerates of NPs, unable to be internalized by cells.

Table 3.2 *NTA results*

Size Distribution	Mean ± Standard error
Mean	159.6 ± 2.9 nm
Mode	49.0 ± 1.1 nm
Standard deviation	108.3 ± 4.3 nm
D10	51.2 ± 0.6 nm
D50	130.3 ± 5.1 nm
D90	311.6 ± 1.8 nm

3.2   Drug loading

Uptake optimization was one of the main focuses of this project. In the beginning, NPs were loaded through a solution 1mM of AGI-6780 in DMSO, but the amount of the encapsulated drug resulted insufficient. In fact, during dialysis and in the time lapse before cell treatment with the NPs in cell viability tests, the loss of drug was shown to be very high (see stability test in Figure 3.10) and the synergistic effect of free CFZ and AGI-6780-loaded NPs was not always clearly visible. For this reason, other loading methodologies were explored. Since AGI-6780 is highly hydrophobic, the idea was to change loading solution, by mixing the drug in a DMSO-water solution. The presence of water molecules in the solution should in fact encourage AGI molecules to enter in the pores and be adsorbed, according to hydrotropic principles, discussed in detail in the following.

First very encouraging results were achieved by loading MSNs in a 1 mM solution of AGI-6780 in a 50-50% volume solution of DMSO and bidistilled water. The amount of drug encapsulated seemed to be extremely higher (more than 50 times), if compared to the values reached with loading in DMSO alone.

The tests on 50-50%DMSO-water loading were interrupted when, during a cell viability test, it was discovered through optical microscopy that in this DSMSO/water volume ratio AGI precipitates in the form of sharp, long rod-like crystals. The absorbance values of the drug loading evaluation were thus completely unreliable, being altered by the presence of the crystals. To better understand the mechanism of AGI precipitation, various solutions of AGI-DMSO-water with fixed amount of AGI but different DMSO/water ratios were prepared and the presence of crystals through microscopy was checked. These analyses showed that only 50/50 volume ratio led to drug precipitation. The loading protocol shifted consequently to 60/40 DMSO/water volume ratio, which guarantees the absence of crystals and allows hydrotropic enhancement of drug loading levels. With this last volume ratio, drug loading was proved to be increased (almost 4 times greater than loading in DMSO), see Table 3.3 and Figure 3.7.
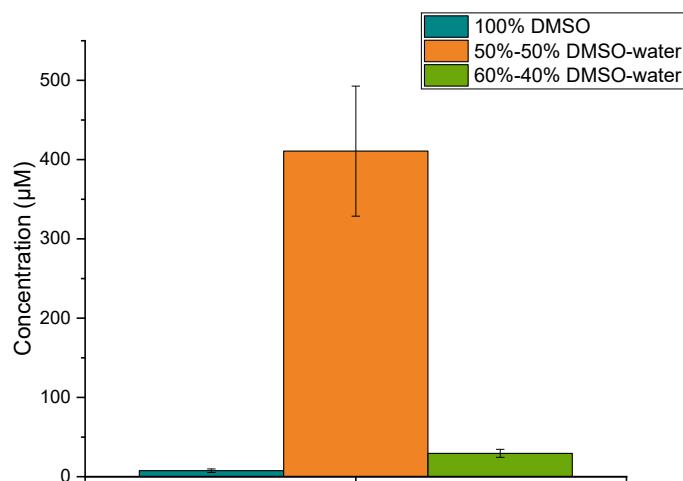

Figure 3.7 *Comparison between AGI loading methods: AGI dissolved in DMSO alone (left) and AGI mixed in 50-50% in volume DMSO-water solution (center) and mixed in 60-40% in volume DMSO-water solution (right).*

Table 3.3 *Comparison between loading values of the three different methods: AGI in DMSO alone, AGI in 50-50% volume DMSO-water solution and AGI in 60-40% volume DMSO/water solution.*

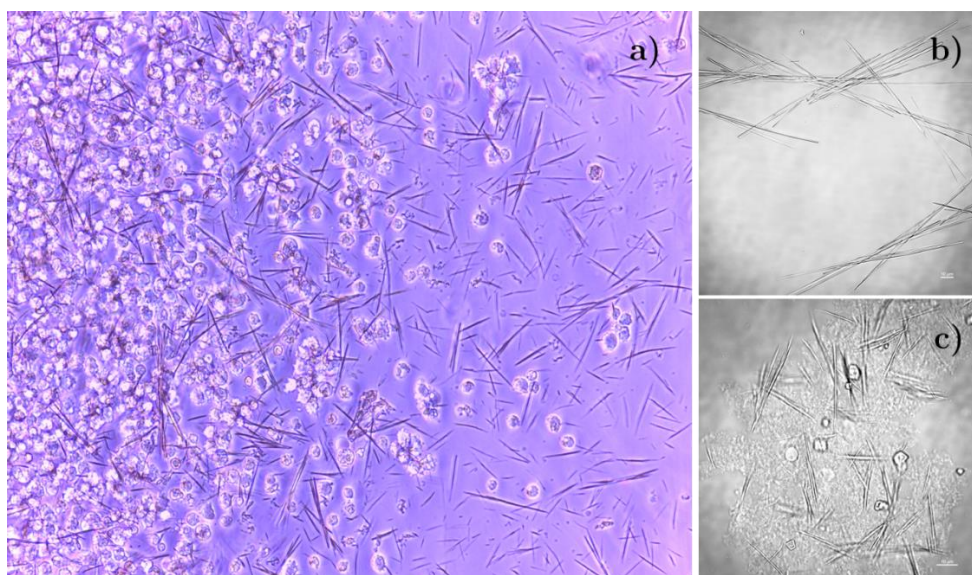|	DMSO (n = 8)	DMSO+H_2O 50-50% (n=7)	DMSO+H_2O 60-40% (n=4)
Concentration (µM)	$7{,}59 \pm 2{,}27$	$410{,}71 \pm 82.02$	$29{,}47 \pm 5{,}09$
Loaded AGI per mg NP (µg)	$1{,}46 \pm 0{,}44$	$79{,}11 \pm 15{,}80$	$5{,}68 \pm 0{,}98$
Loading efficacy (%)	$0{,}76 \pm 0{,}23$	$41{,}07 \pm 8{,}20$	$2{,}95 \pm 0{,}51$

Figure 3.8 *Microscopy images of AGI-6780 precipitates, generated by mixing AGI in a 50%-50% DMSO-water solution. A) AGI precipitates in a cell culture. AGI precipitates identified in a DMSO-water-AGI solution (B) and in a loaded-NPs solution (C).*

Hydrotropy

Hydrotropy is a technique used to enhance the water solubility of highly hydrophobic molecules by the addition of a second solute, called hydrotrope or chaperon molecule. Hydrotropes are small amphiphilic molecules, whose hydrophobic part interact with the poorly water-soluble molecule whereas the hydrophilic part helps the solubilization in water. It is known that hydrotrope-assisted solubilization of

hydrophobic substances is concentration dependent, showing a typical sigmoidal solubility curve. At low concentrations of hydrotropes, in fact, the solubility does not change evidently; beyond a certain concentration threshold, called minimum hydrotrope concentration, solubilization of the poor water-soluble molecule significantly increases. The sudden enhancement of solubility is caused by the self-aggregation of the hydrotropes, which happens in that concentration conditions [43].

In the specific case of this work, it is possible that the enhancement of drug loading with the addition of water in the solution, it is indeed due to hydrotropy effect: DMSO could in fact work as a chaperon molecule, having a short-chain amphiphilic structure. The interaction between H_2O and DMSO molecules is still not clear; however, Rajesh et Al., by monitoring the presence of Hydrogen Bonds (HB) with FTIR analysis in DMSO-water solution at different concentrations, hypothesized the presence of four distinct species of DMSO in water (Figure 3.9): Free form, forming no HB with H_2O molecules, 1HB (single HB with H_2O molecules), 2HB (a single molecule of DMSO binds to 2 molecules of H_2O) and the A aggregate form, in which DMSO molecules interact with each other. The population of DMSO species was seen to vary with the concentration of DMSO, having first a preferential interaction with water molecules (majority of 1HB and 2HB forms) until 35% mol DMSO. At higher concentration the favorite form is the aggregate one [44]. This could be a possible explanation of the enhanced loading efficacy of 60/40%-DMSO/water volume ratio solution. The DMSO molecules, according to these authors, should in fact present mainly in the aggregate form, being in the above-mentioned hydrotrope self-aggregation condition which enhances the solubility of poor water-soluble molecules (AGI-6780 in this case).
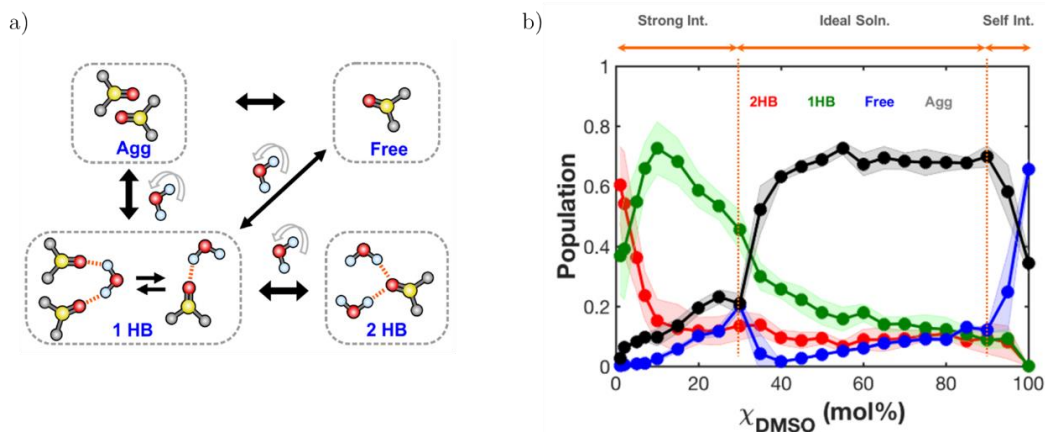
Figure 3.9 *a) DMSO species present in DMSO/water binary mixtures: Aggregate, Free, 1 Hydrogen Bond, 2 Hydrogen Bonds. b) population of DMSO species as a function of DMSO concentration in water* [44].

3.3   Stability tests and Release tests

Stability and release test were performed to evaluate the behaviour of NPs in the storage buffer (PBS) and culture media, respectively. The ideal condition would be when all the encapsulated drug remains in the pores of MSNs until the internalization of NPs in the target cells. Every leakage happening in the storage solution or in the culture media should be considered a loss, which decreases the therapeutic efficacy of the nanoparticles. Results are shown below according to the MSNs loading protocol followed.

Stability and Release tests with AGI-loaded NPs in 100% DMSO

In the case of NPs loaded in DMSO alone, stability test in PBS showed that already in the first hours, AGI leakage is significant; in fact, absorbance values exceeded the ones of the starting solution, suggesting the loss of the totality of the drug (Figure 3.10, left panel). Nevertheless, in vitro test (described in the following paragraphs) showed a good efficacy of the AGI-loaded NPs, indicating that an effective amount of drug is still present in the NPs at the moment of cell treatment. These stability test and in vitro test results are inconsistent, and more tests should be done to better quantify drug leakage before cell culture. A possible explanation can reside in the indirect nature of the evaluation method for both the loaded and the lost drug.

Better results were obtained for the release tests in RPMI, where no leakage of drug was highlighted by UV-vis analysis (Figure 3.10, right panel). This could be due to the fact that in RPMI are present a varied population of proteins, which may surround the lipid-coated nanoparticles, helping the lipidic shell to maintain the drug inside the MSNs.
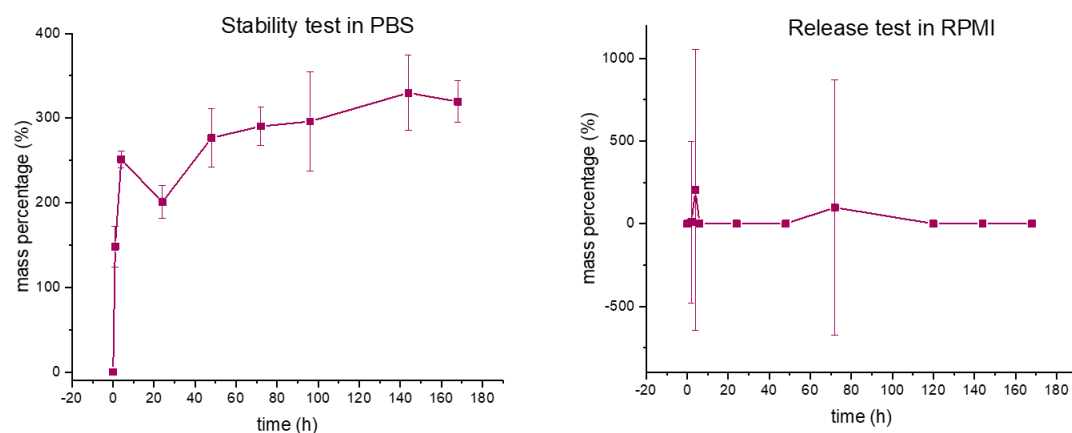
Figure 3.10 *Stability (left) and release (right) test performed on lipid-coated MSNs, loaded with the first method (AGI dissolved in DMSO alone). On the vertical axes is represented mass percentage, i.e., the percentage of estimated drug present in the solution or in RPMI, with respect to the starting amount of loaded drug.*

Stability and Release tests with NPs loaded in 50%-50% DMSO-water

After having proved the great loss of AGI encapsulated in MSNs with the DSMO-alone loading method, stability and release test were performed for MSNs loaded with the 50%-50% DMSO-water solution. The results of these tests are unfortunately not reliable, due to the presence of AGI precipitates altering absorbance values of UV-vis spectroscopy analysis, as previously discussed.
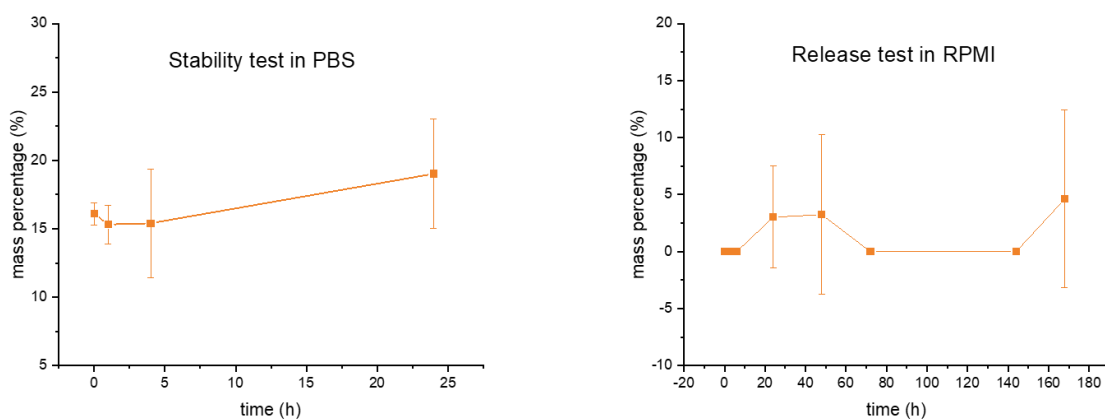

Figure 3.11 *Stability (left) and release (right) test performed on lipid-coated MSNs, loaded with the second method (AGI dissolved in 50%-50% DMSO-water solution).*

On the vertical axes is represented mass percentage, i.e., the percentage of estimated drug present in the solution or in RPMI, with respect to the starting amount of loaded drug.

3.4   In vitro tests

To evaluate the cytotoxicity of the NPs and their synergy with the free proteasome inhibitor CFZ, cell viability tests were performed on a human MM cell line, KMS-28. AGI-6780-loaded MSNs and empty MSNs (control samples) were covered with lipids, dialyzed, and administered to the cells in culture with two possible concentrations: 50 µg/mL or 25 µg/mL. The 2 or 6 hours after the treatment (depending on the protocol followed) with NPs, the cells were treated with 2.5 nM free CFZ. Cell viability was evaluated by FACS analysis at prefixed time points. The weakness of all these tests is the lack of repetitions: a minimum of 3 test with identical protocols should be performed to consider the results statistically valuable.

In parallel with NPs tests, the evaluation of the synergistic cytotoxic effect of AGI-6780 with CFZ was performed, treating the cells with free AGI-6780 5 µM and successively with CFZ. The results are considered as standard to compare with the results of in vitro test with NPs treatments. From the Figure 3.12, the synergistic effect of free AGI and CFZ is clearly visible, reaching a peak during day 3 from the starting of treatment (only 14.3% cells alive). It is also notable that AGI alone in the concentration used is not harmful for the cells. CFZ alone is cytotoxic (more than 50% cells are killed within day 2) but its effect is potentiated by the presence of AGI. In both CFZ and CFZ+AGI samples a trend can be noted: the lowest viability is located at day 3; in the following days, the cells have the tendency to recover, and the viability heightens.
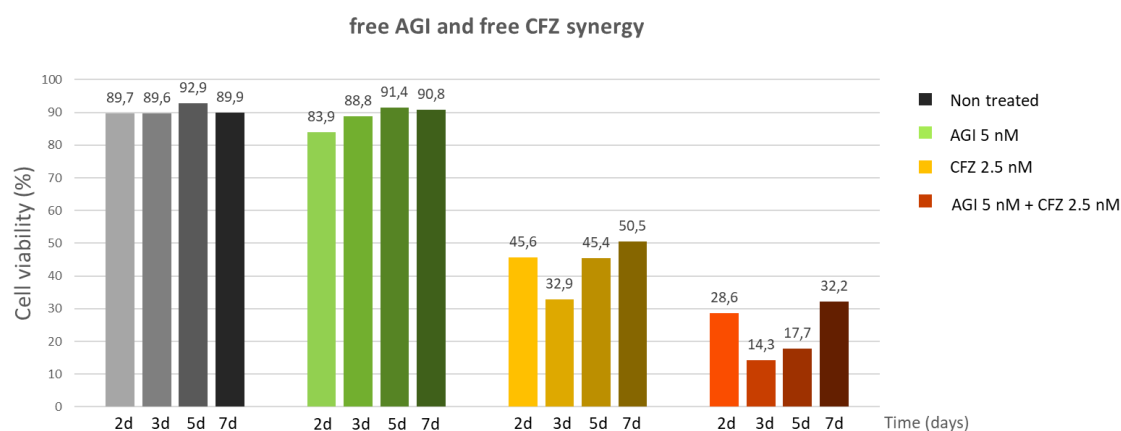
Figure 3.12 *Cell viability test results: treatment with free AGI and free CFZ to verify the synergistic effect of combined drugs on MM-cells.*

In vitro test with NPs loaded in 100% DMSO

Several test, with different protocols were carried out in order to optimize the KMS-28 cells treatment steps and to better evaluate the synergistic effect of the AGI-loaded NPs and free CFZ. In the following, are reported the most representative and encouraging results and for each presented experiment, the results are shown in terms of percentage of viable cells, together with a summary of the passages followed. In general, despite the results of stability test, which suggested that in the hours preceding cell treatment with the NPs a considerable drug leakage occurs, the majority of the viability tests clearly showed the effect of the cytotoxic synergy produced by loaded NPs in combination with free CFZ. In fact, the mortality of the cells treated with both loaded NPs and CFZ tends to be notably superior to the one produced by CFZ alone and even more so by loaded NPs alone. These tests demonstrated that an effective amount of drug menages to reach the cells, visibly inducing apoptosis in the MM cells. This first results are encouraging, as they refer to NPs loaded through the less efficacious method; increasing the amount of loaded AGI, the synergistic lethal effect is expected to enhance and give more stable results in terms of cell viability after the combined treatment.

NP8 experiment (Figure 3.133) was performed seeding cells and treating them with NPs (both empty and AGI-loaded NPs, concentrated 25 µg/mL) at time 0. CFZ (2.5 nM) was administered after 2 hours, and cell viability was evaluated after

48h through FACS analysis. The mortality of the cells is higher for the NPs-CFZ combined treatment, (only approximately 50% cells viable), showing the presence of the synergistic effect of the NPs-carried AGI and CFZ.
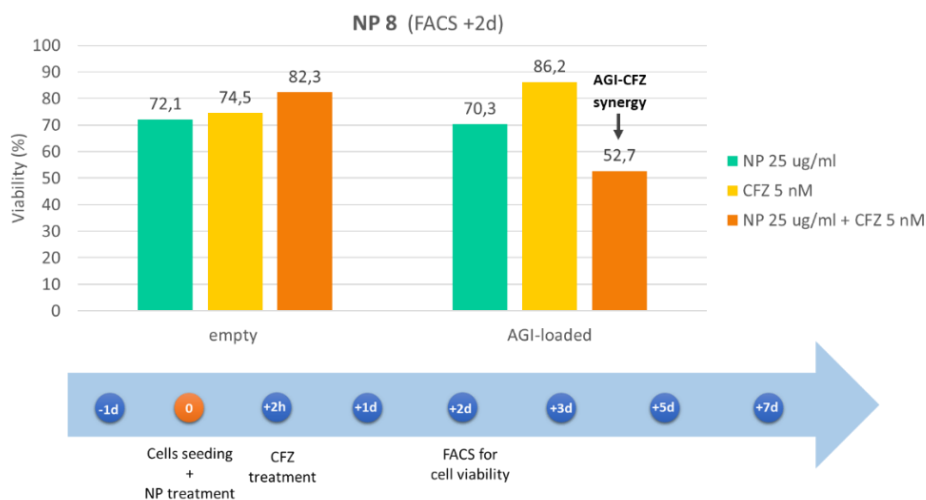

Figure 3.13 *NP8 viability test results.*

NP9 steps are identical of the ones followed in NP8 test, except that FACS analysis were performed at day 5 instead of day 2. The synergy is here more visible (Figure 3.14) than in the previous experiment: the viability of cells at day 5 (31.1%) is lower than the one measured at day 2 in NP8 test (52.7%), indicating that the cytotoxic effect of NPs in combination with CFZ persist in time and increases after day 2, reducing cell viability by almost a factor of 3.
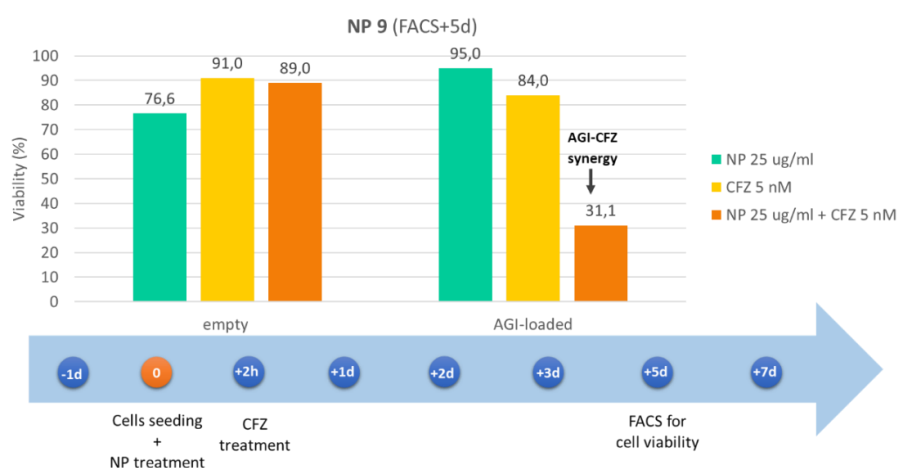

Figure 3.14 *NP9 viability test results*

NP11 test was conducted with a double CFZ administration: cells were seeded and treated with NPs at time 0 and CFZ was administered after 2 hours and 72 hours. FACS analysis was performed at day 5, as in NP9 test. A completely treatment-free sample (marked in black in Figure 3.15) was introduced as control standard for cell viability. Also in this test the mortality is remarkably higher for cells treated with both NPs and free CFZ, confirming the synergistic effect, but no sign of effects of the double CFZ treatment are visible.
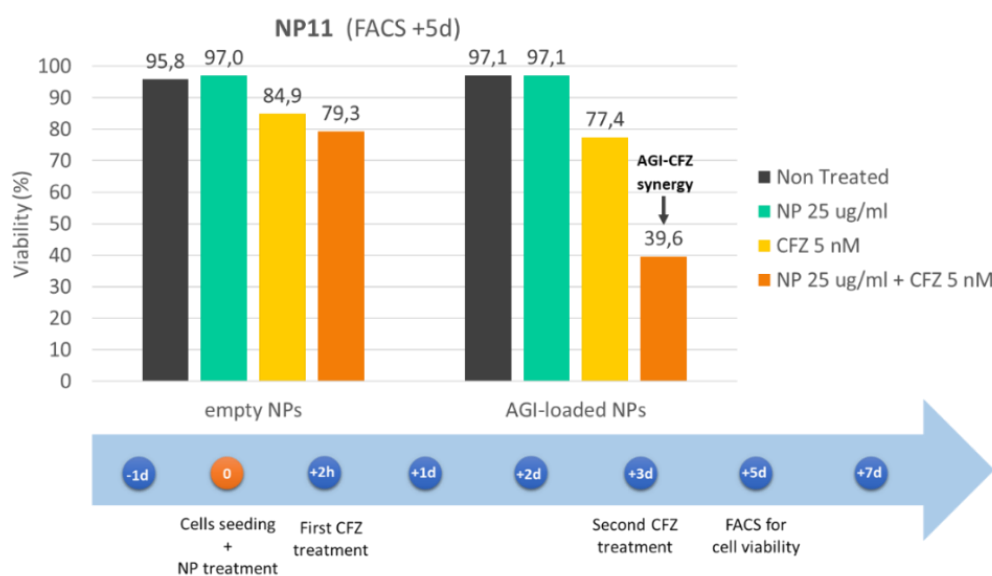

Figure 3.15 *NP11 viability test results*

The effect of a double NPs treatment was explored in test NP12 in which the cells were seeded at day -1 (time zero coincides with the second treatment with NPs, to allow the comparison between protocols with double and single NP treatments) and treated the first time with NPs. The second NPs administration was performed after 24 hours, and viability of cells was evaluated 7 days after this second NP treatment. In this experiment, a further concentration of NPs (50 µg/mL) was tested beyond the 25 µg/mL one. From the results (Figure 3.16) it is evident that the synergistic effect of the nanocarried AGI and free CFZ is strongly present even after a week, giving proof of the efficacy of the NPs. Thus, NP effect persists in time, suggesting a slow and continuous drug release, which is fundamental to achieve a drug concentration in the therapeutic window. From NP12 results is visible that the higher NPs concentration is more efficient in terms of cell mortality

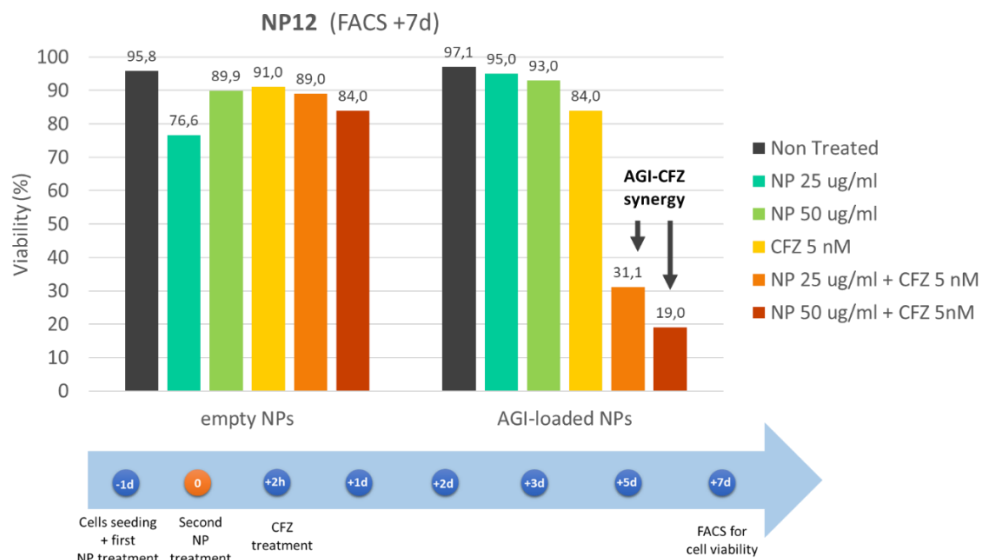than the lower concentration (19.0% vitality of cells treated with 50 µg/mL NPs against 31.1% with 25 µg/mL).

Figure 3.16 *NP12 viability test results*

In vitro test with NPs loaded in 50%-50% DMSO-water

Cell viability test were performed also for NPs loaded in 50%-50% DMSO-water solution, with the idea that NPs would have encapsulated a higher amount of drug and would have enhanced the mortality of the cells. It was during these tests that the presence of AGI precipitates was noted, bringing into question the results concerning the drug loading evaluation, the stability, and the release tests obtained for NPs loaded with this method. Nonetheless, interesting information can be extracted from the viability test results, which in this case were more complete, as FACS data were collected more frequently (2, 3, 5 and 7 days after the initial treatment) allowing to follow the time evolution of the cell viability.

The reported test are NP15 and NP16 (Figure 3.17), which showed a synergistic effect, similar to the one observed for the free drugs synergy tests, demonstrating that in the NPs carried an effective amount of AGI. Similarly to free AGI treatment, the after a peak in mortality at day 3, cells have the tendency to recover, with the only exception of cells treated with 50 µg/mL and CFZ in NP15. This could be due

to the fact that the drug may be carried minimally by the NPs, being present in cell culture in the form of AGI crystals, which can generate on cells an effect analogous to the free-AGI one. In both test, cell viability is mostly reduced by the free CFZ combined with the higher concentration of NPs (50 µg/mL), according with the results obtained in NP12 test. It is notable that even empty NPs produce an enhanced cytotoxicity when combined to CFZ treatment. This is possibly because NPs presence could help the CFZ to enter the cells, enhancing its efficacy.

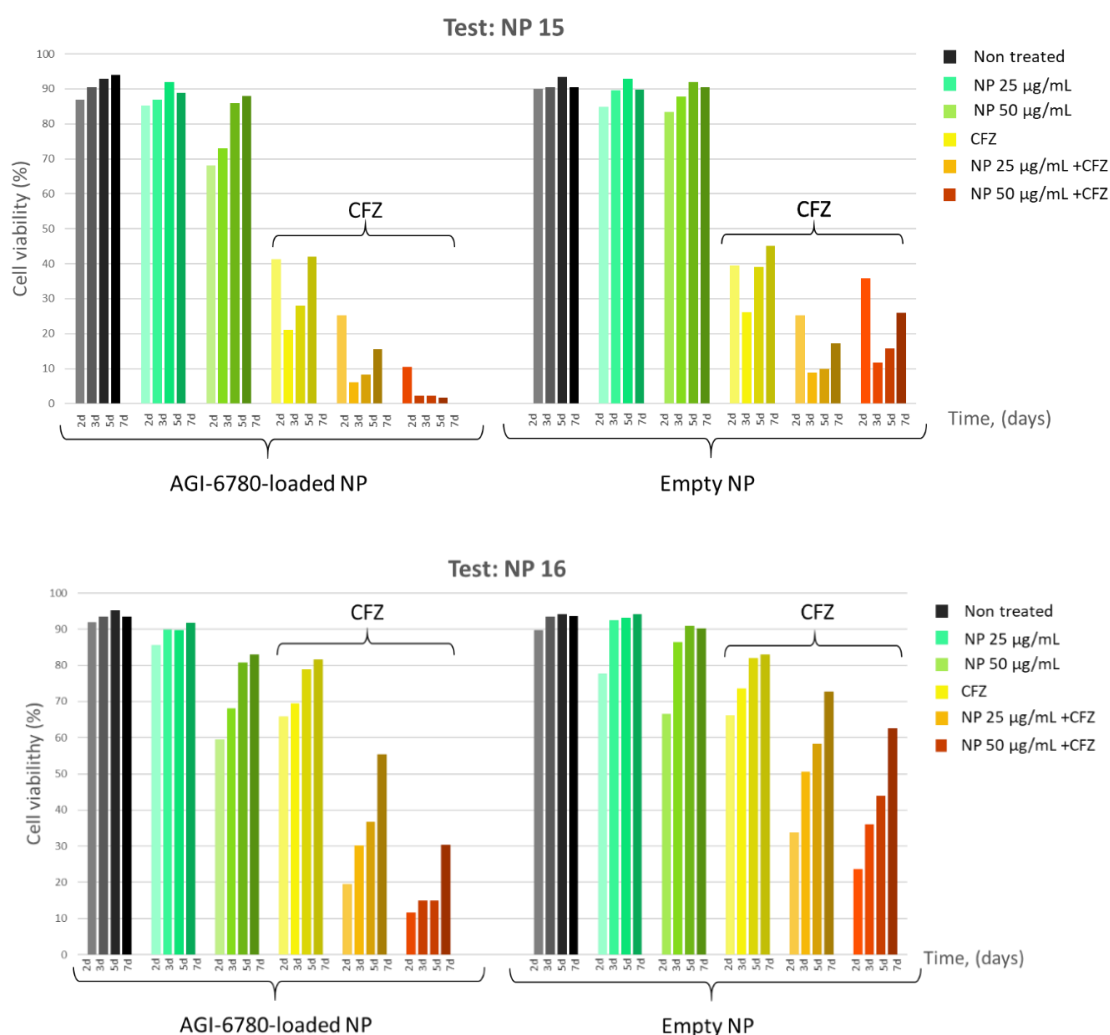**Figure 3.17** *NP15 and NP16 Viability test results: time evolution of the effect of AGI-loaded NPs (two concentration tested: 25 µg/mL and 50 µg/mL) alone and in combination with free CFZ (2.5 nM) - left side of the graphs - ; in comparison with empty NPs (two concentration tested: 25 µg/mL and 50 µg/mL) alone and in combination with free CFZ (2.5 nM)- right side of the graphs.*

3.5 Fluorescence microscopy and colocalization analysis

Fluorescence microscopy analysis was performed on lipid-coated MSNs, in order to evaluate the efficacy of the coupling between MSNs and the lipidic bilayer. A rough estimation of the number of the coated MSNs is in fact given from the colocalization tool, which counts separately the fluorescent spots corresponding to MSNs and lipids (labelled with two different dyes) and then counts the spots coinciding in the merged image of MSNs and lipids channels. In the images reported (Figure 3.18), MSNs were labelled with Atto 647 (far red channel, pink in the images) and the lipids were labelled with DiO (green channel). In particular, the analyses were carried out before (figure a,b,c) and after dialysis (figure d, e, f), to assess the presence of improvements in MSNs coating. Colocalization analysis results confirmed the beneficial effect of the dialysis, showing an enhancement in the average colocalization percentages from 52% before dialysis to 84% after dialysis (percentages refer to the number of colocalized spots, in relation to the total of MSNs spots).
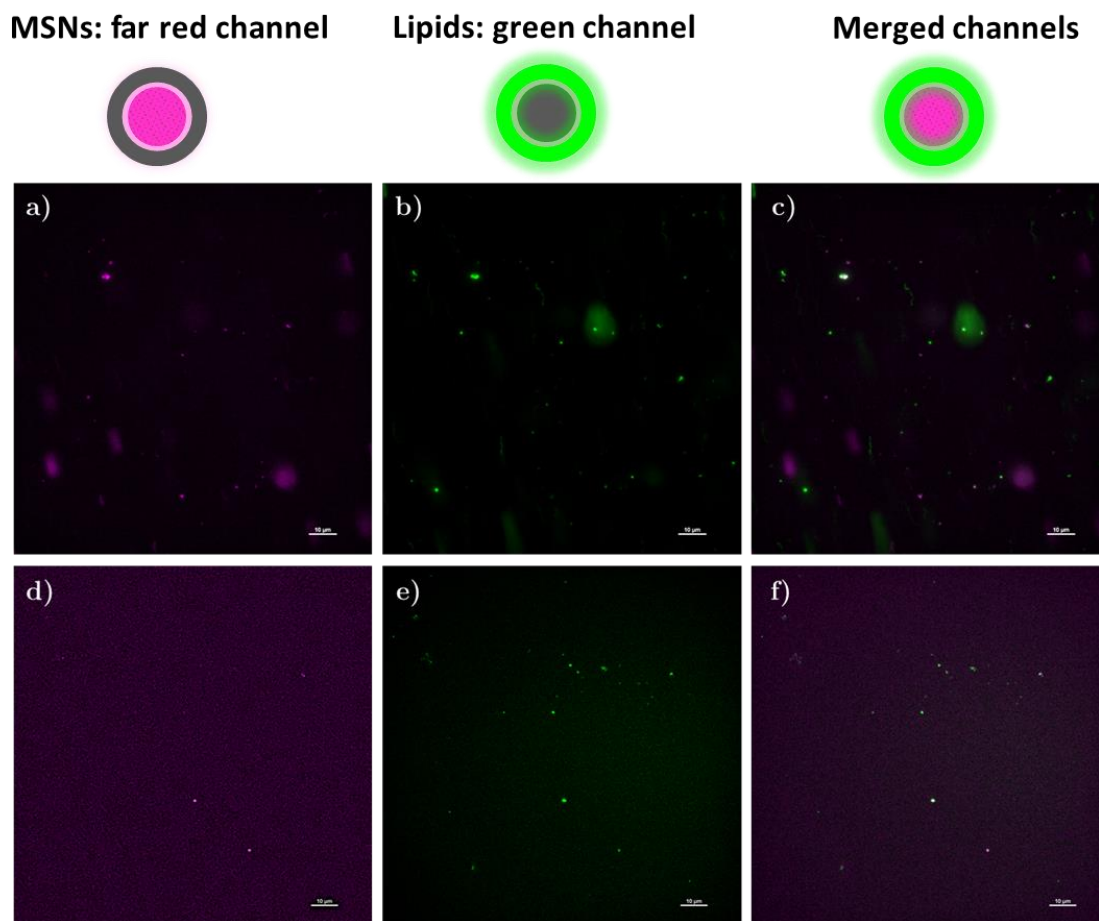
Figure 3.18 *Fluorescence microscopy images of lipid-coated MSNs before (a, b, c) and after (d, e, f) dialysis. Atto 647-labelled MSNs are visible in far red channel (left: a, d); DiO-labelled lipids are visible in the green channel (center: b, e) and the merged channel are presented in the right side (e, f).*

3.6   Hemocompatibility tests

The hemocompatibility test was performed twice. From the plots there is a clear difference between control samples (not coagulated) and samples treated with CaCl$_2$, which coagulated in different moment. It is in fact clearly visible that plasma and plasma together with physiological solution or coated MSNs showed similar behaviour and same coagulation times, whereas coagulation for uncoated MSNs samples happened earlier.

These results indicate that lipid bilayer coating is fundamental for hematological compatibility of the nanoparticles. They can also be seen as demonstration that a good and stable lipidic coverage of MSNs was achieved. The two tests showed notably similar results, suggesting a good repeatability of the test.

Coagulation time (t_c) was calculated as the time point corresponding to the central absorbance point (a_c), calculated as follows:

$$a_c = \min\ a\ + \frac{\max\ a\ - \min\ a}{2}$$

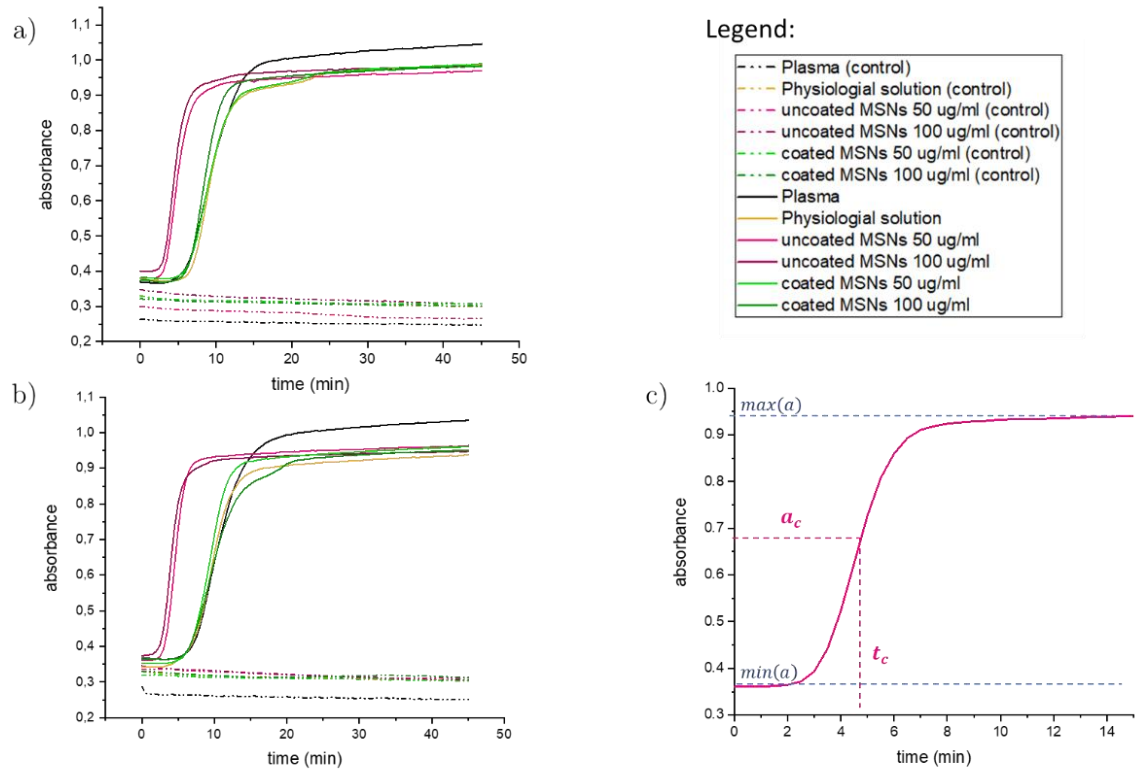Where a is the vector of the absorbance values of the sample.

Figure 3.19 *Results from test n.1 (a) and from test n.2 (b). Representation of coagulation time computing method (c).*

Table 3.4 *Coagulation time results.*

	t_c test 1 (min)	t_c test 2 (min)	Mean ± st.dev (min)
Plasma	9,67	10,75	**10,21±0,76**
Physiological solution	9,45	9,81	**9,63±0,26**
Uncoated MSNs 50 µg/ml	4,98	4,68	**4,83±0,21**
Uncoated MSNs 100 µg/ml	4,63	4,12	**4,37±0,36**
Coated MSNs 50 µg/ml	9,26	9,52	**9,39±0,19**
Coated MSNs 100 µg/ml	8,76	10,24	**9,50±1,05**

3.7 Functionalization

Gel electrophoresis

Gel electrophoresis was performed on non-reduced Daratumumab (sample A) and on TCEP-reduced Daratumumab (sample B) to verify the antibody rupture, through the evaluation of the molecular weights (MW) of the fragments. Entire Daratumumab is expected to have, as every monoclonal antibody, a MW of approximately 150 kDa. To assess the molecular weight of the loaded samples, a marker (M), which contains pre-stained and highly purified proteins with precise MW ranging from 10 to 250 kDa, was also loaded in the gel. From the picture reported in Figure 3.20, it is visible that for sample A (non-reduced Daratumumab) a single band formed around 150kDa, while for sample B (reduced Daratumumab) multiple bands appeared, confirming the fragmentation of the antibody. A particularly intense band, near 150kDa, could be attributable to Daratumumab still not reduced, the other bands could represent the population of different-weighted fragments of the antibody (Figure 3.21Figure 3.21). Considering that light chains and heavy chains composing the antibody structure have respectively MW around 25 kDa and 50 kDa, and that TCEP acts on disulphide bonds holding together the chains, it can be hypothesized that the band near 100 kDa may be produced by the central part of the antibody i.e, the two heavy chains together, the band at 75 kDa may derive from the antibody split in the middle (a heavy and a light chain together) and the bands at 50 kDa and 25 kDa could be related to single heavy and light chains respectively.
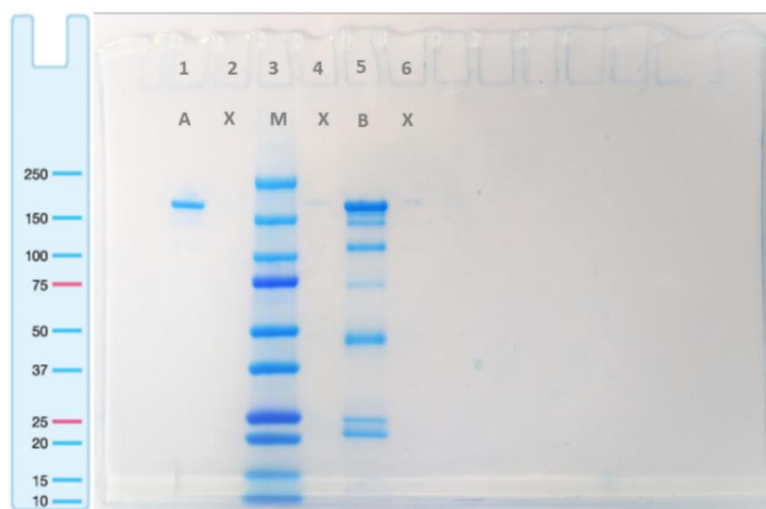
Figure 3.20 *SDS-PAGE results: picture of the gel after staining with Comassie blue and washing (right). Sample A is non-reduced Daratumumab, sample B is Daratumumab reduced with TCEP, and M is the marker (Precision Plus standard, BioRad). Precision Plus standard marker reference for 4-15% Criterion-TGX gel by BioRad (left); scale unit is kDa.*
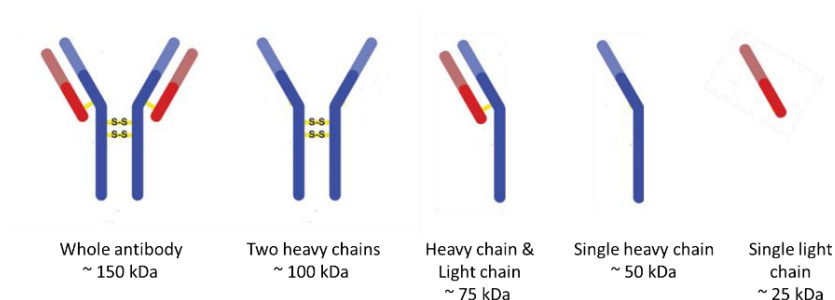
Figure 3.211 *Antibody and antibody fragments population, with their relative estimated molecular weight.*

Fluorescence analysis

Fluorescence microscopy analysis were performed at the end of the antibody binding process as proof of concept. The aim was visualizing through a multichannel analysis if lipid-coated MSNs were actually functionalized, and the nanoconstruct correctly assembled.

For the first functionalization test, MSNs were colored with Atto 550 (red channel) or with Atto 647 (far red channel) and their coating with DiD (far red channel)

and DiO (green channel) respectively. A Coumarin-bond secondary antibody was used to label the antibody fragments, since it selectively interacts with the Fab region of the antibody, guaranteeing specificity towards Daratumumab fragments. Unfortunately, the nanoparticles amount was very low: samples with Atto 647-labelled MSNs and DiO-labelled lipids were barely visible; however, samples with Atto 500-labelled MSNs and DiD-labelled lipids, although with weak signals, showed encouraging signals of colocalization in the three channels.

To confirm these results, a second test was made employing a higher amount of NPs and antibody. In this case, a control sample without functionalization was prepared and processed exactly as the functionalized one, except for the antibody binding step. Control sample and functionalized one were both treated with coumarin-secondary antibody complex, which interacted selectively with Daratumumab fragments exposed by the NPs of the functionalized sample. Fluorescence analysis of control sample and functionalized sample were performed before and after a washing procedure (including centrifugation and resuspension of the pelleted NPs). As shown by Figure 3.222, in the case of functionalized sample, coumarin (bule channel) is visible both before and after the washing step, whereas in the control sample coumarin is not visible (Figure 3.23). This represents a proof that the antibody-DSPE-PEG-maleimide was efficiently incorporated in the lipidic shell, because otherwise the antibody fragments would have been removed by centrifugation and coumarin would have not been visible after sample washing.

Colocalization analysis of the images was performed and colocalization percentage was calculated for the 3 channel merged images and for the three channel couples: MSNs-lipids, MSNs-antibodies; lipids-antibodies (see Table 3.1). For each condition, a total of 10 images were elaborated and the resulting colocalization values were averaged, obtaining the colocalization percentages. The results are very promising, since more than 50% of MSNs spots are coincident to both lipids and antibody ones. Also colocalization percentages relative to couples of channels are very high; in particular, for MSNs and lipids, the value in very similar and thus consistent with the value obtained (84%) for the fluorescence analysis of lipid coated MSNs reported in paragraph 3.5. Colocalization decreases after centrifugation step, which eliminates the non-bound antibody fragments.

Table 3.5 *3 channel colocalization analysis results.*

	MSNs + lipids + Antibody / MSNs	MSNs + lipids / MSNs	MSNs + Antibody / MSNs	lipids + Antibody / Antibody
Pre-Centrifuge (n=10)	63,5%	86,0%	82,8%	80,0%
Post-Centrifuge (n=10)	53,5%	80,0%	61,2%	62,6%

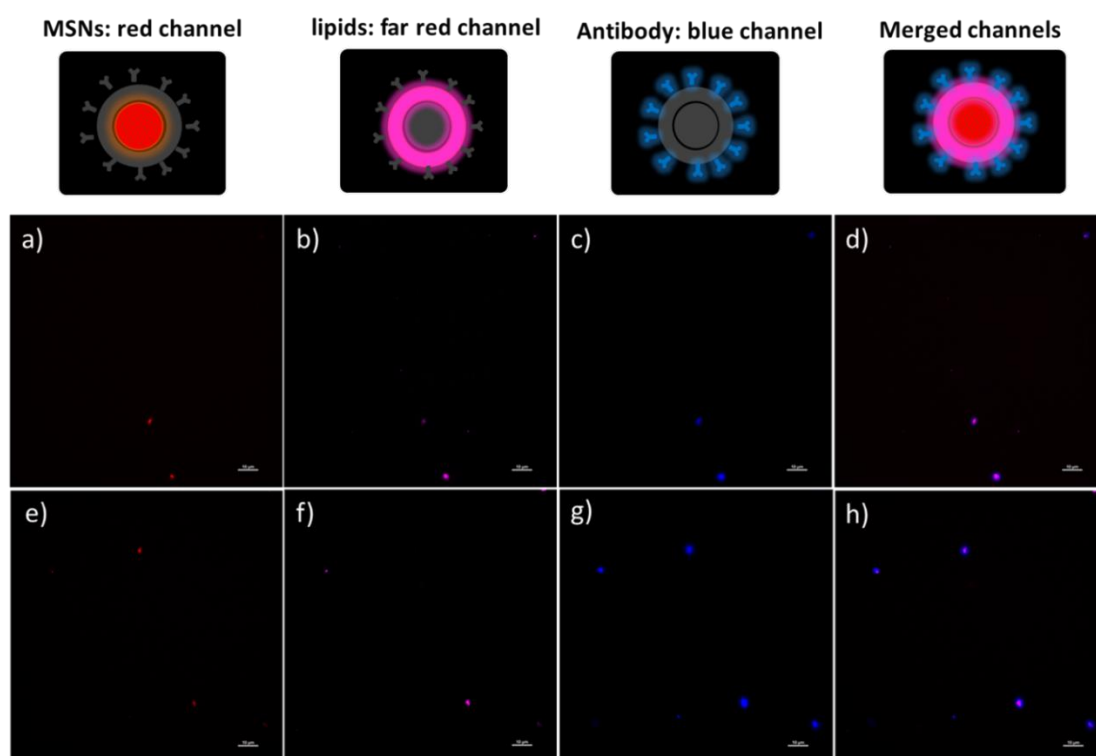**Figure 3.22** *Fluorescence microscopy images of functionalized, lipid-coated MSNs before (a, b, c, d) and after (e, f, g, h) dialysis. Atto 550-labelled MSNs are visible in the red channel (a, e); DiD-labelled lipids are visible in the far-red channel (b, f); Daratumumab labelled with the secondary antibody-coumarin complex is visible in the blue channel (c, g); and the merged channels are presented in the right side (d, h).*
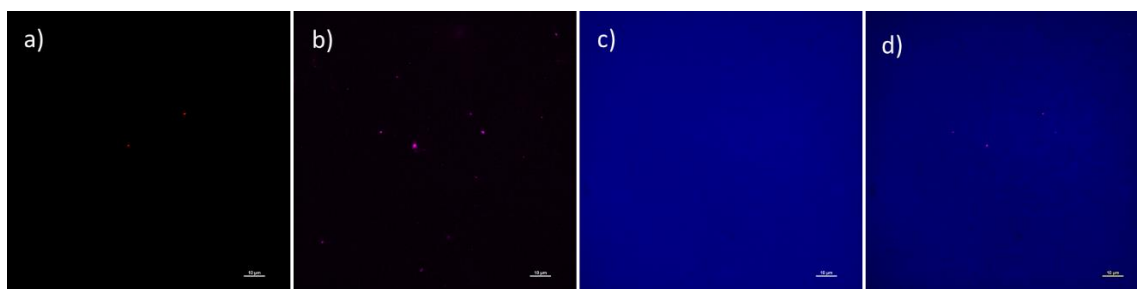
Figure 3.23 *Fluorescence microscopy images of non-functionalized, lipid-coated MSNs after dialysis. Atto 550-labelled MSNs are visible in the red channel (a); DiD-labelled lipids are visible in the far-red channel (b); blue channel does not show any fluorescent spot, but only a blue background since Daratumumab is not present. The merged channels are presented in the right side (d).*

4 Conclusions and future perspectives

In this Master Thesis work, an initial phase was dedicated to the characterization of the developed mesoporous silica-based nanocarriers, which confirmed the data collected in previous works: MSNs, with huge surface area and mesoporous structure are an ideal material as nanocarrier core. In fact, MSNs demonstrated evident ability to host a great amount of IDH2 inhibitor AGI-6780, which is dramatically hydrophobic and impossible to administer through conventional modalities. MSNs cores offer therefore the opportunity to expand the selection of possible therapies to employ in the fight against multiple myeloma.

Self-assembled lipid bilayers were produced on the silica core from a previously optimized DOPC-Chol-DSPE-PEG-mixture following a consolidated protocol, which includes the solvent exchange technique, giving rise to a biomimetic core-shell structure, called protocell. Zeta potential analysis confirmed the good colloidal stability conferred to the nanocarriers by the lipidic shell, which is also necessary to allow surface functionalization for active targeting, prevent premature leakage of the drug and improve the biocompatibility as well as the pharmacokinetics of the nanoparticles. With this regard, extremely interesting results were achieved in this work with hemocompatibility tests: while uncoated MSNs generated anticipated plasma coagulation, lipid-coated MSNs behaved similarly to physiological solution, demonstrating the fundamental role of the lipidic coating. Moreover, hemocompatibility test offered indirectly the evidence that an effective MSNs coating was achieved. This last assertion is consistent with fluorescence microscopy analysis, where MSNs and lipid resulted coincident in space with percentage higher than 80%. Colocalization analysis on coated MSNs hence confirmed the correct assembly of the nanoparticles, also demonstrating the utility of the dialysis process, which, beyond NPs purification from exceeding drug, helps the formation of a cohesive lipidic shell on the MSNs core. Colocalization percentages were in fact found to increase from approximately 50% before dialysis to 84% post-dialysis.

In this work, several aspects of the project were carried out in parallel. Firstly, new MSNs loading methods were explored, relying on hydrotropy principles, and an optimized loading solution was found in AGI dissolved in a 60%-40% DMSO-water solution. The amount of loaded drug was brought from approximately 1.5 μg to 5.7 μg per mg MSNs, almost quadruplicating the loading.

Secondly, stability and release test were carried out for 100% DMSO and 50-50% DMSO-water loading method, giving however uncertain results: in the first case, the amount of lost drug seems to be too high if compared to the amount of encapsulated drug, suggesting that AGI molecules remaining in the core at the moment of cell treatment with NPs is extremely low. In the second case, evidence of drug precipitation in form of crystals was found, demonstrating that this loading method is impracticable. Further studies and test are necessary to evaluate the stability and the release profile of NPs loaded with the 60%-40% DMSO-water solution.

In vitro cell viability tests were performed as proof of concept of the correct loading of the NPs. In general, these tests consolidated the evidence of AGI-6780 and CFZ synergy and confirmed the effectiveness of the NPs as nanocarriers. Mortality percentages over 80% were reached for the loaded-NPs and the free CFZ combination. However, the tests performed lack of statistical validity and need to be repeated. Moreover, proof of the effective endocytosis of NPs is still needed (cytofluorimetry analysis), as well as cell viability tests, including treatment with the NPs loaded with the 60%-40% DMSO-water solution is missing.

The main weakness of the developed nanocarriers is yet the lack of size homogeneity. This is particularly highlighted by NTA analysis, which shows a wide distribution of hydrodynamic radiuses, indicating the presence of big NPs agglomerates that might compromise cell internalization. To solve this problem, size selection of NPs is needed. A possible strategy could be the employment of an extruder for liposomes, whose membranes should act as a sieve for MSNs, contextually covering them with lipids.

Another step forward was achieved in this work for what concerns functionalization and active targeting: the therapeutic human monoclonal antibody Daratumumab, was successfully reduced into fragments and conjugated to DSPE-PEG-maleimide, which was successively fused in the lipidic shell of the NPs. 3-channel fluorescence microscopy analysis provided a proof of the correct assembly of the nanocarriers and the presence on their surface of targeting antibody fragments. The colocalization percentage reached are in fact extremely promising, suggesting to proceed with in vitro test assessing the efficacy of the highly selective ability of the active targeting moieties against MM cells.

To conclude, although some uncertainties, data and evidences collected pave the way for the development of a truly effective nanosized, highly biomimetic delivery system, externally decorated with specific monoclonal antibody and capable of selective targeting against multiple myeloma. Encouraging results were achieved, demonstrating once more the immense potential of nanomedicine, which offers innovative and smart therapeutic perspectives to improve MM and, more in general, cancer patient prognosis.

References

[1]   S. Gori *et al.*, "I numeri del cancro in Italia," *Rep. AIOM-AIRTUM*, pp. 1–232, 2020.

[2]   S. K. Kumar *et al.*, "Multiple myeloma," *Nat. Publ. Gr.*, vol. 3, 2017, doi: 10.1038/nrdp.2017.46.

[3]   G. Talamo *et al.*, "Beyond the CRAB Symptoms: A study of presenting clinical manifestations of multiple myeloma," *Clin. Lymphoma, Myeloma Leuk.*, 2010, doi: 10.3816/CLML.2010.n.080.

[4]   S. Asher and M. J. Streetly, "Myeloma and MGUS," *Medicine (United Kingdom)*. 2021, doi: 10.1016/j.mpmed.2021.02.009.

[5]   D. E. Joshua, P. Joy Ho, J. Gibson, and R. D. Brown, "The immune system in myeloma," in *Multiple Myeloma and Related Disorders*, 2004.

[6]   C. Caprio, A. Sacco, V. Giustini, and A. M. Roccaro, "Epigenetic aberrations in multiple myeloma," *Cancers (Basel).*, vol. 12, no. 10, pp. 1–16, 2020, doi: 10.3390/cancers12102996.

[7]   M. A. Dicato, "Multiple myeloma," in *Side Effects of Medical Cancer Therapy: Prevention and Treatment: Second Edition*, 2018.

[8]   Y. Yang, "Cancer immunotherapy: Harnessing the immune system to battle cancer," *Journal of Clinical Investigation*. 2015, doi: 10.1172/JCI83871.

[9]   D. Bianca, "End-on Covalent Antibody Immobilization on Dual Polarization Interferometry Sensor Chip for Enhanced Immuno-sensing Methods to Design and Synthesize Antibody-Drug Conjugates (ADCs) Reduction - Alkylation Strategies for the Modification of Specific Monoc," pp. 8–11.

[10]   P. de la Puente and A. K. Azab, "Nanoparticle delivery systems, general approaches, and their implementation in multiple myeloma," *Eur. J. Haematol.*, vol. 98, no. 6, pp. 529–541, 2017, doi: 10.1111/ejh.12870.

[11]   K. Okazuka and T. Ishida, "Proteasome inhibitors for multiple myeloma," *Jpn. J. Clin. Oncol.*, vol. 48, no. 9, pp. 785–793, 2018, doi: 10.1093/jjco/hyy108.

[12]   M. A. Dimopoulos *et al.*, "Carfilzomib and dexamethasone versus bortezomib and dexamethasone for patients with relapsed or refractory multiple myeloma (ENDEAVOR): And randomised, phase 3, open-label, multicentre study," *Lancet Oncol.*, 2016, doi: 10.1016/S1470-2045(15)00464-7.

[13]   S. Gandolfi, J. P. Laubach, T. Hideshima, D. Chauhan, K. C. Anderson, and P. G. Richardson, "The proteasome and proteasome inhibitors in multiple myeloma," *Cancer Metastasis Rev.*, 2017, doi: 10.1007/s10555-017-9707-8.

[14]   J. Almond and G. Cohen, "The proteasome: a novel target for cancer

chemotherapy," pp. 433–443, 2002, doi: 10.1038/sj/leu/2402417.

[15] K. Tanaka, "The proteasome: Overview of structure and functions," *Proc. Japan Acad. Ser. B Phys. Biol. Sci.*, vol. 85, no. 1, pp. 12–36, 2009, doi: 10.2183/pjab.85.12.

[16] L. Kubiczkova, L. Pour, L. Sedlarikova, R. Hajek, and S. Sevcikova, "Proteasome inhibitors - molecular basis and current perspectives in multiple myeloma," *J. Cell. Mol. Med.*, 2014, doi: 10.1111/jcmm.12279.

[17] V. T. de M. Hungria *et al.*, "New proteasome inhibitors in the treatment of multiple myeloma," *Hematology, Transfusion and Cell Therapy*, vol. 41, no. 1. Elsevier Editora Ltda, pp. 76–83, Jan. 01, 2019, doi: 10.1016/j.htct.2018.07.003.

[18] R. Piva and E. Bergaggio, "IDH2 inhibition enhances proteasome inhibitor responsiveness in hematological malignancies." 2019.

[19] E. B. Roberto Piva, "Wild-Type IDH Enzymes as Actionable Targets for Cancer Therapy," *Cancers (Basel).*, vol. 11, no. 11, p. 563, 2019, doi: 10.1001/archotol.1971.00770060940019.

[20] S. Tommasini-Ghelfi, K. Murnan, F. M. Kouri, A. S. Mahajan, J. L. May, and A. H. Stegh, "Cancer-associated mutation and beyond: The emerging biology of isocitrate dehydrogenases in human disease," *Sci. Adv.*, 2019, doi: 10.1126/sciadv.aaw4543.

[21] W. Yu, K. E. Dittenhafer-Reed, and J. M. Denu, "SIRT3 protein deacetylates isocitrate dehydrogenase 2 (IDH2) and regulates mitochondrial redox status," *J. Biol. Chem.*, vol. 287, no. 17, pp. 14078–14086, 2012, doi: 10.1074/jbc.M112.355206.

[22] R. Narayan, U. Y. Nayak, A. M. Raichur, and S. Garg, "pharmaceutics Mesoporous Silica Nanoparticles: A Comprehensive Review on Synthesis and Recent Advances," doi: 10.3390/pharmaceutics10030118.

[23] M. Conte, "Multifunctional Immunocompatible Nanotheranostics particles for pancreatic cancer," no. December, 2020.

[24] R. Vinhas, R. Mendes, A. R. Fernandes, and P. V. Baptista, "Nanoparticles-Emerging potential for managing leukemia and lymphoma," *Frontiers in Bioengineering and Biotechnology.* 2017, doi: 10.3389/fbioe.2017.00079.

[25] B. Dumontel, "Development and biostability evaluation of hybrid nanoconstructs for cancer therapy based on zinc oxide nanocrystals," no. November, 2020.

[26] P. Moriarty, "Nanostructured materials," *Reports Prog. Phys.*, vol. 64, no. 3, pp. 297–381, Mar. 2001, doi: 10.1088/0034-4885/64/3/201.

[27] F. Hoffmann, M. Cornelius, J. Morell, and M. Fröba, "Silica-based mesoporous organic-inorganic hybrid materials," *Angewandte Chemie - International Edition*. 2006, doi: 10.1002/anie.200503075.

[28] N. T. Chen, S. H. Cheng, J. S. Souris, C. T. Chen, C. Y. Mou, and L. W. Lo, "Theranostic applications of mesoporous silica nanoparticles and their organic/inorganic hybrids," *J. Mater. Chem. B*, 2013, doi: 10.1039/c3tb20249f.

[29] V. Cauda *et al.*, "Colchicine-loaded lipid bilayer-coated 50 nm mesoporous nanoparticles efficiently induce microtubule depolymerization upon cell uptake," *Nano Lett.*, vol. 10, no. 7, pp. 2484–2492, 2010, doi: 10.1021/nl100991w.

[30] V. Cauda, A. Schlossbauer, and T. Bein, "Bio-degradation study of colloidal mesoporous silica nanoparticles: Effect of surface functionalization with organo-silanes and poly(ethylene glycol)," *Microporous Mesoporous Mater.*, 2010, doi: 10.1016/j.micromeso.2009.11.015.

[31] Y. Chen, H. Chen, and J. Shi, "In vivo bio-safety evaluations and diagnostic/therapeutic applications of chemically designed mesoporous silica nanoparticles," *Advanced Materials*. 2013, doi: 10.1002/adma.201205292.

[32] P. N. Durfee *et al.*, "Mesoporous Silica Nanoparticle-Supported Lipid Bilayers (Protocells) for Active Targeting and Delivery to Individual Leukemia Cells," *ACS Nano*, vol. 10, no. 9, pp. 8325–8345, 2016, doi: 10.1021/acsnano.6b02819.

[33] B. A. Zannetti *et al.*, "Novel Insights in Anti-CD38 Therapy Based on CD38-Receptor Expression and Function: The Multiple Myeloma Model," *Cells*, 2020, doi: 10.3390/cells9122666.

[34] N. W. C. J. van de Donk *et al.*, "Monoclonal antibodies targeting CD38 in hematological malignancies and beyond," *Immunological Reviews*. 2016, doi: 10.1111/imr.12389.

[35] H. M. Shepard, G. L. Phillips, C. D. Thanos, and M. Feldmann, "Developments in therapy with monoclonal antibodies and related proteins," *Clin. Med. J. R. Coll. Physicians London*, vol. 17, no. 3, pp. 220–232, 2017, doi: 10.7861/clinmedicine.17-3-220.

[36] A. Bertero, "Tesi di Laurea Magistrale Biomimetic drug delivery nanosystem for a targeted approach against multiple myeloma," 2020.

[37] N. Hosen *et al.*, "CD48 as a novel molecular target for antibody therapy in multiple myeloma," *Br. J. Haematol.*, 2012, doi: 10.1111/j.1365-2141.2011.08941.x.

[38] L. Malavasi, *Structural characterization techniques: Advances and applications in clean energy.* 2016.

[39] W. Zhou, R. Apkarian, Z. L. Wang, and D. Joy, "Fundamentals of scanning electron microscopy (SEM)," *Scanning Microsc. Nanotechnol. Tech. Appl.*, pp. 1–40, 2007, doi: 10.1007/978-0-387-39620-0_1.

[40] A. Connelly, "BET surface area," *Laboratory Techniques, Science.* 2017.

[41] M. Marino, "Biomimetic mesoporous silica nanoparticles for drug delivery in a synthetic lethality approach," 2018.

[42] E. Joseph and G. Singhvi, "Multifunctional nanocrystals for cancer therapy: A potential nanocarrier," in *Nanomaterials for Drug Delivery and Therapy*, 2019.

[43] W. Chen *et al.*, "Facile Strategy Enabling Both High Loading and High Release Amounts of the Water-Insoluble Drug Clofazimine Using Mesoporous Silica Nanoparticles," *ACS Appl. Mater. Interfaces*, vol. 10, no. 38, pp. 31870–31881, Sep. 2018, doi: 10.1021/acsami.8b09069.

[44] C. B. Kavya Rajesh , Kwang-Im Oh, "uderstanding DMSO/water interactions," vol. 35, no. 2004, p. 15343, 2015.